# $\begin{array}{c} \text{Modeling of dielectrophores is in micro and} \\ \text{nano systems} \end{array}$

by

Yuan Lin

May 2008 Technical Reports from Royal Institute of Technology KTH Mechanics SE-100 44 Stockholm, Sweden Akademisk avhandling som med tillstånd av Kungliga Tekniska Högskolan i Stockholm framlägges till offentlig granskning för avläggande av teknologie doktorsexamen onsdagen den 11:e Juni 2008 kl<br/> 10:00 i Sal D2, Kungliga Tekniska Högskolan, Lindstedtsvägen 5, Stockholm. ©Yuan Lin2008Universitetsservice US–AB, Stockholm 2008

## Modeling of dielectrophoresis in micro and nano systems

#### Yuan Lin 2008

KTH Mechanics SE-100 44 Stockholm, Sweden

#### Abstract

This thesis presents models and simulations of dielectrophoretic separation of micro and nano particles. The fluid dynamics involved and the dielectric properties of water inside single-walled carbon nanotube are studied as well.

Based on the effective dipole moment method, the particle dynamic model focuses on the translational motions of micro particles. The hydrodynamic force between the particles and the particle-particle electrostatic interactions are considered as well. By comparing the dimensionless parameters, the dominating force can be determined. Based on a simplified version of the particle dynamic model, two numerical simulations are carried out to predict the efficiency of dielectrophoretic separation of micro size particles. The first calculation suggests a strategy to improve the trapping efficiency of *E.coli*. bacteria by applying superimposed AC electric fields. The second calculation discusses the concept of mobility and improves the separation rate of particles by a multi-step trapping-releasing dielectrophoresis strategy.

The model is extended down scale to calculate the separation of metallic and semiconducting single-walled carbon nanotubes by the modified effective dipole moment method for prolate ellipsoids. The steeply changed gradient of electric field results in the local joule heating therefore creates gradient of dielectric properties in the solution. As a result, certain pattern of fluid flow with a considerable strength is created and affects the motion of carbon nanotubes especially close to the electrode gap, which indicates that the so-called electrothermal flow should be considered in designing the experiment to separate single-walled carbon nanotubes.

When the length scale of particles is comparable to that of the electrodes, the calculation of dielectrophoretic force by the effective dipole moment is considered not to be accurate since only the electric field in the center point is taken into account. Hence in the thesis a new method based on distributed induced charge is suggested. By approximating a straight slender body as a prolate ellipsoid, the electric field of multiple points along the centerline are all considered in the calculation and the interaction between particles could be concurrently taken care. This method is expected to be an improved method to calculate the dielectrophoretic force of rod-like virus, DNA, nanowires and carbon nanotubes.

The dielectric property of water confined in carbon nanotubes is expected to be dramatically different from that of bulk water. The thesis also contains

a molecular dynamics study to reveal the difference also a dependence on the diameter of carbon nanotubes. The results show that along the axial direction, both the static permittivity and the relaxation time are larger than the isotropic bulk water, and in the cross-section plane it is opposite. When the radius of the carbon nanotubes increases, the properties of water inside become closer to the bulk water.

#### ${\bf Descriptors:}$

Dielectrophoresis, micro particle, molecular dynamics, single-walled carbon nanotubes, hydrodynamics, particle-particle interaction, superimposed, multi-step, electrothermal flow, SPC/E, water, Brenner

#### **Preface**

This thesis contains the following papers:

- **Paper 1** Aldaeus, F., Lin, Y., Roeraade, J. & Amberg, G. 2005 Superpositioned dielectrophoresis for enhanced trapping efficiency *Electrophoresis 26* 4252-4259 (2005)
- **Paper 2** Aldaeus, F., Lin, Y., Amberg, G & Roeraade, J. 2006 Multi-stepped dielectrophoresis for separation of particles *J. Chromatography A* 1131 261-266 (2006)
- Paper 3 Lin, Y., Amberg, G., Aldaeus, F. & Roeraade, J. 2006 Simulation of dielectrophoretic motion of microparticles using a molecular dynamics approach *Proceedings of ASME ICNMM 2006-4th International Conference on Nanochannels, Microchannels and Minichannels (2006)*
- **Paper 4** Lin, Y., Shiomi, J., Maruyama, S. and Amberg, G. 2007 Electrothermal flow in dielectrophoresis of single-walled carbon nanotubes *Physical Review B*, 76 045414(1-5)(2007)
- Paper 5 Lin, Y., Shiomi, J. and Amberg, G. 2008 Numerically calculate dielectrophoretic force of slender body to be submitted
- **Paper 6** Lin, Y., Shiomi, J., Maruyama, S. and Amberg, G. 2008 Dielectric properties of water inside single-walled carbon nanotubes to be submitted

Related papers, not included in this thesis

- Lin, Y., Amberg, G. 2006 Simulation of dielectrophoresis of finite size particles Proc. 2nd International Conference on Transport Phenomena in Micro and Nanodeviese, Barga Italy, June (2006)
- Lin, Y., Shiomi, J., Maruyama, S., Amberg, G. 2007 Fluid dynamics in dielectrophoresis separation of carbon nanotubes *Japanese Fluid Dynamics Meeting*, *Tokyo*, *Japan*, *August* (2007)

May 2008, Stockholm

Yuan Lin

#### Division of work between authors

- Paper 1, Yuan Lin (YL) developed the code and carried out the calculation with the feedback from Gustav Amberg (GA) and Fredrik Aldaeus (FA). The writing was done by FA with feedback from YL, Johan Roeraade (JS) and GA.
- Paper 2, The development of code and the simulation are carried out by YL with the feedback from GA and FA. The writing was done by FA with feedback from YL, JS and GA.
- Paper 3, YL performed the development of code and carried out the simulation with the feedback from GA. The experiment result is performed by FA and JS. The writing part was done by YL with feedback from GA. FA and JS revised the paper.
- Paper 4, The coding and calculation and the writing of the paper were performed by YL with feed back from Junichiro shiomi (JS) and GA. JS revised the paper with feed back from Maruyama Shigeo (MS) and GA.
- Paper 5, Modeling was performed by YL with feedback from GA and JS. YL carried out the coding. The calculation and writing of this paper were done by YL with feedback from JS and GA.
- Paper 6, YL inherited the molecular dynamics code from JS and MS and carried out the Ewald summation for periodic boundary condition and parallelized the code. The calculation and writing of this paper were done by YL with feedback from JS, MS and GA.

# Contents

Abstra	act	iv		
Prefac	е	v		
Chapte	Chapter 1. Introduction			
Chapte	er 2. Theoretical preliminaries	7		
2.1.	Governing equations of incompressible fluids	7		
2.2.	Basic concepts in electrostatics	7		
2.3.	Effective dipole moment	9		
2.4.	Basic molecular dynamics simulation	14		
Chapte	er 3. Modeling and numerical treatment	18		
3.1.	Particle dynamics method	18		
3.2.	Fluid dynamics in micro and nano systems	22		
3.3.	Modeling of DEP based on distributed charge density	24		
3.4.	Ewald summation	26		
Chapte	er 4. Simulation results	30		
4.1.	Superimposition of dielectrophoretic forces	30		
4.2.	Multi-step dielectrophoresis	30		
4.3.	Inter-particle dielectrophoretic forces	32		
4.4.	Electrothermal flow in DEP separation of SWNTs	33		
4.5.	Calculation of DEP force on a slender body	35		
4.6.	Dielectric properties of water inside SWNTs	35		
Chapter 5. Conclusions and outlooks				
Ackno	wledgements	41		
Bibliog	graphy	42		

# Part I Overview and summary

#### CHAPTER 1

## Introduction

In 1958, scientists developed the first trial silicon chip [Helvajian (1999)]. By arranging a huge number of microscopic transistors onto a single silicon chip, microelectronic circuits could be built and remarkable improvements in all aspects are achieved. This led to the Information Revolution. Later on, researchers found that mechanical devices can also be miniaturized and batchfabricated, promising the same benefits to the mechanical world, which results in the strong trend towards miniaturizing equipment for chemical analysis and synthesis until today [Karniadakis & Beskok (2001)]. The obvious advantages are lower cost consumption, shorter response time, less pollution, better process control etc. This trend is strengthen by the development of lithography based microtechnology, which fabricates laboratory functions on a single chip of only few millimeters to centimeter in size. This is the Lab-on-a-chip (LOC) concept, and is often indicated as *Micro Total analysis system* as well. Recently, as nanotechnology progresses, research in LOC systems is extended towards fluid handling of nanoparticles as single-walled carbon nanotubes (SWNTs), proteins, DNA and virus [Krupke et al. (2003a); Kadaksham et al. (2005); Dimaki & Bøggild (2004); Morgan & Green (1997)]

Essentially being a field dedicated to the miniaturization of pumping and fluidic manipulation, microfluidics offers the possibility of solving these issues in biology and chemistry fields. The fundamental fluid physics of fluid systems change rapidly when the length scale decreases. For example, the most well-known phenomenon is that gravity becomes negligible but surface tension plays an important role. Also the momentum transport in microfluidic devices is dominated by viscous dissipation and the inertial effect is generally negligible, which diminishes the instabilities caused by the nonlinearity of inertia. However, on the other hand, many other phenomena of physics and chemistry become prominent such as electrostatics, thermodynamics, elasticity etc., which greatly enriches the field of microfluidics [Morgan & Green (2003); Karniadakis & Beskok (2001); Asbury & Engh (1998); Morgan & Green (1997)].

As one of the earliest applications of microfluidic devices, separation and deposition of cells and particles with small size differences, constantly attract great research interest in analytical chemistry. Various strategies based on different principles are employed, i.g., mechanical (filters, micropipettes,

1

#### 2

etc), magnetical, optical and electrical (electro-osmosis, electrophoresis, dielectrophoresis) separation methods. Each method has its own advantages and disadvantages and is therefore suitable for certain application field. This thesis studies the issues related to dielectrophoresis (DEP) approach since the particles we have interest to separate (bio-cells, carbon nanotubes) have close sizes and different frequency dependent electric properties which makes them difficult to separate by other methods.

A neutral polarizable particle suspended in a fluid with different polarizabilitiy experiences a DEP force in a non-uniform field (it can be a DC or an AC field) due to the induced charges. Particles are attracted to the regions of stronger electric field when their permittivity  $\epsilon_p$  exceeds that of the suspending medium  $\epsilon_m$ , i.e., when  $\epsilon_p > \epsilon_m$ , and the DEP force in this case is called positive DEP. On the other hand, particles are repelled from regions of stronger electric field when  $\epsilon_p < \epsilon_m$  and the DEP force is called negative DEP. Figure 1.1 shows a dielectric sphere experiencing a positive DEP in a DC field. The direction of the DEP force is independent of the direction of electric field, therefore it does not matter the electric field is DC or AC.

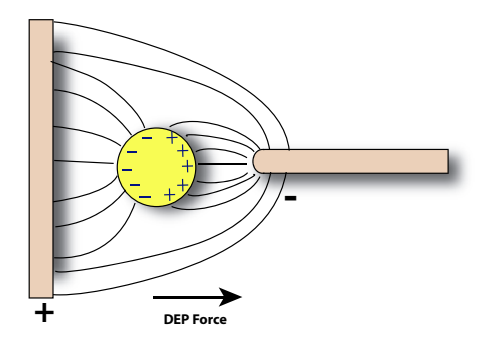


FIGURE 1.1. A schematic of a particle suspended within a point-plane electrode system. When the particle polarizes, the interaction between the dipolar charges with the local electric field produces a force.

An increasingly important application of DEP is the selective separation of bio-particles in LOC systems, and the feasibility has been demonstrated for a variety of cells. For example, Pohl (1975) carried out the separation of viable and non-viable yeast cells, and later he extended the experiments to separate other biological particles including canine thrombocytes, red blood cells, bacteria etc. Becker and colleagues [Becker et al. (1995)] performed a separation of human breast cancerous cells from normal blood cells by a microelectrode array due to the large difference in dielectrophoretic properties of those cells. Moreover, Gascoyne and associates [Gascoyne et al. (1997)] managed to separate various cancerous cells from blood cells and normal murine erythrocytes

from erythroleukemia cells and measured their dielectric properties by changing the frequency of the applied electric field. Markxa and colleagues [Markx et al. (1996)] separated a mixture of bacteria Bacillus subtilis, E. coli bacteria and Micrococcus luteus.

There are several commonly used strategies for the DEP separation in LOC systems. One is the flow separation. That is, a flow is used to carry two types of different particles in a microchannel. One type of particles is trapped on the electrode arrays located at the bottom of the channel, and the other type would be brought out of channel by the flow. It has been demonstrated to be effective for separation of cancer cells [Becker et al. (1995)]. The disadvantage of this strategy is that the cells attracted to electrodes need to be collected after the separation. Therefore, strategies combining the separating and collecting processes are of interest recently.

Dielectrophoretic-field flow fractionation (DEF-FFF) is another strategy in which a carrier flow is introduced with different speeds at different heights from the bottom surface. Particles are repelled from the electrodes under a negative DEP force. The particles with different dielectric properties would be found at different heights and therefore travel at different speeds with the flow. For example, Markxb and colleagues [Markx et al. (1997)] employed this method in the separation of latex particles with different sizes, and Yang and associates [Yang et al. (1999)] performed the separation of human breast cells mixture with blood cells. DEP-FFF makes use of the velocity gradient in the flow profile to achieve a high selective separation. However, the particles probably enter the channel with a Gaussian-shaped distribution which may cause overlap between the sub-populations of particles after separation.

Traveling wave DEP (TW-DEP) is another recent and popular strategy in which electric fields rather than flow is used to give the particles a mean longitudinal velocity. Several applied electric fields are applied with continuous phase shift to give particles DEP forces in both vertical and horizontal directions. TW-DEP has been demonstrated to separate erythrocyte and leukocyte cells [Morgan et al. (1997); Green et al. (2002)].

In recent years, a lot of research has been done in DEP manipulation of a variety of nanoparticles [Green & Morgan (1999)], nanorods, nanofibers, deoxyribonucleic acid [Washizu & Kurosawa (1990)], viruses [Morgan & Green (1997)], proteins [Washizu et al. (1994)] and DNA [Asbury & Engh (1998)]. More recently, DEP was used to separate metallic and semiconducting SWNTs [Krupke et al. (2003a); Krupke et al. (2003b); Krupke et al. (2004)] and depose metallic SWNTs to form thin film [Krupke et al. (2006)] and use semiconducting SWNTs to fabricate electric transistors as well [Zhang et al. (2005); Zhang et al. (2006)].

However, when the scale extends to nanosystems, other effects become significant in DEP system besides Brownian motion of the particles. For example

#### 4 1. INTRODUCTION

the usage of high electric field strengths produces fluid flow and heating of the suspending electrolyte. The electric field can interact with the fluid to produce frequency dependent forces such as electro-osmosis and electrothermal force [Green et al. (2002); Ramos et al. (1998); Lin et al. (2007)]. The resulting flow exerts a drag force on the particles and produces an observable motion. Recently, a new type of force has been observed on microelectrodes due to the electric double layer (EDL) of the surface of electrodes in an AC electric field [Ramos et al. (1998); Morgan & Green (2003)]. The EDL around particle is also believed to enhance the DEP effects on submicron particles and a simple model which combines EDL effect into the effective dipole moment is described in Morgan & Green (2003). A thorough investigation of models related to EDL around a particles was done by Lyklema (1995).

Since the manufacture of microsystems is costly and the measuring is time-consuming, numerical modeling and simulation is essential and efficient to predict the motion of the particle under DEP forces therefore to optimize the design of experiments. Most of the previous simulations utilize the effective dipole moment based models suggested by Jones (1995). Combined with the distributed Lagrange multiplier method suggested by Glowinski and colleges to solve Navier Stokes equations, DEP motion of microparticles and nanoparticles were simulated [Glowinski et al. (2001); Kadaksham et al. (2004); Kadaksham et al. (2005)]. A numerical study using DEP forces combined with uniform channel flow to separate metallic and semiconducting SWNTs was carried done by Dimaki & Bøggild (2004), where the effective dipole moment method for prolate ellipsoids are used.

However, the assumption of an effective dipole moment is, the size of particle should be far below the characteristic length of the electric field. If it is not true, two methods are suggested which provide solution with higher accuracy than the effective dipole moment method. One is the Maxwell stress tensor (MST) method [Wang et al. (1997); Singh & Aubry (2007)], and the other is the multipole moment method [Washizu (1992); Washizu & Jones (1994); Jones & Washizu (1996); Jones (1995); Washizu (2004); Liang et al. (2004)]. The equivalence of this two methods has been demonstrated analytically [Wang et al. (1997)] and numerically [Rosales & Lim (2005)]. However, the computational cost of both methods is high since by the MST method, numerical integration around the particle surface needs to be done and by the multipole moment method, high order derivatives of the electric field needs to be calculated. This makes them impractical to simulate several interacting particles, which is a typical situation in real separation systems. Besides, multipole moment method is not available for particles rather than spherical shape.

In any case, numerically calculating the electric field is essential and which can be typically done by finite element method or boundary element method. Rosales & Lim (2005) performed a DEP calculation for sphere and ellipsoid by MST method based on boundary element method. By boundary element

method, there is a full matrix need to solve, therefore the memory requirement is demanding. Singh & Aubry (2007) reported a study of transport and deformation of droplets using DEP by finite element and levelset methods. FemLego [Amberg et al. (1999)] and Comsol Multiphysics are finite element toolboxes for user-defined partial differential equations, and DEP-solver developed by Rosales & Lim (2005) provides a choice based on boundary element method.

In this thesis, the accepted effective dipole method has been used to model and simulate manipulation and separation of  $E.\ Coli$  bacteria, micro-size latex beads, and SWNTs. A study of the electric field-driven electrothermal fluid flow in DEP separation of SWNTs is also reported. Considering manipulating rod-shaped nano-wires, DNA fragment, virus and carbon nanotubes by DEP force, the effective dipole moment method is not so accurate for calculation since the length of particles is comparable to that of the electrodes. A model based on induced charge density is suggested in this thesis to numerically calculated the DEP force and torque of a highly elongated straight slender body. This method is expected to provide higher accuracy than the effective dipole moment method and its computation is still rather simple. The basic idea is to assume that the induced charges concentrated on the centerline of the slender body, therefore, by enforcing the boundary conditions, a one-dimensional integral equation system is obtained with induced charge densities as unknowns.

A molecular dynamics (MD) study of water molecules confined in carbon nanotubes is also presented in this thesis, since water-filled carbon nanotubes are expected to play a central role in future nanoscale devices, for proton storage and transport applications [Mann & Halls (2003)]. Water in a confined SWNTs dramatically changes its dynamic and dielectric properties, which attracts a huge amount of research interests. When the scale extends down to nanoscale, it is reasonable to use MD methods instead of continuum methods to study the fluid [Allen & Tildeslley (1987); Sadus (1999)]. Many free MD packages are currently available, for example AMBER (Assisted Model Building and Energy Refinement) is popular particularly for proteins, nucleic acids and carbohydrates [Pearlmana et al. (1995)], and DL\_POLY is a general purpose serial and parallel MD simulation package [Todorov & Smith (2006)].

Although the principle of MD is simple, the most challenging task of MD is to model the potentials. For example, water is an apparently simple molecule (H<sub>2</sub>O) but with a highly complex character. Although it is usually regarded as a typical liquid, actually it is a unique liquid which has many abnormal properties to fill the requirements of life. Many models have bee developed to discover the structure and properties of water. In a recent review paper of Guillot (2002), 46 models of water are listed. This indirectly indicates their lack of success in a general sense. However, simple models may provide some useful insights. For example, the extended single point charge (SPC/E) model we employed is known for reproducing accurate dielectric constant and potential energy [Watanabe & Klein (1989)].

#### 6 1. INTRODUCTION

The dielectric properties of bulk water have been extensively studied [Anderson et al. (1987); English & Macelroy (2002); Marti et al. (1994)]. MD studies of water confined in graphite channels, on surface of SWNT bundles and inside SWNTs were studied by Marti and colleagues [Marti et al. (2006), Gordillo & Marti (2003); Marti & Gordillo (2002); Marti & Gordillo (2001)], where the carbon nanotubes were modeled as a rigid tubes. In this thesis, the MD study is performed to investigate the anisotropic dielectric properties of water inside both rigid SWNTs and flexible SWNTs and the dependence on diameter, length and density are discussed as well.

#### CHAPTER 2

# Theoretical preliminaries

This chapter outlines some basic principles of micro fluid mechanics, electrostatics and molecular dynamics concerned.

#### 2.1. Governing equations of incompressible fluids

For an incompressible fluid, the governing equation is the Navier-Stokes equation which takes the non-dimensional form as [kundu],

$$\frac{\partial \mathbf{u}}{\partial t} + \mathbf{u} \cdot \nabla \mathbf{u} = -\nabla p + \frac{1}{Re} \nabla^2 \mathbf{u} + \mathbf{f}, \qquad (2.1)$$

where  $Re = \frac{UL}{\nu}$ , and  $\mathbf{u}$ , p and  $\mathbf{f}$  denote velocity, pressure and the external force respectively. In micro and nano systems where the Reynolds number is much less than 1, the nonlinear terms can be neglected and the governing equation is the Stokes equation which takes the form as [Morgan & Green (2003)]

$$\frac{\partial \mathbf{u}}{\partial t} = -\nabla p + \frac{1}{Re} \nabla^2 \mathbf{u} + \mathbf{f}.$$
 (2.2)

Due to the linearity in  ${\bf u}$  of the Stokes equation, it is analytically easier to handle than the Navier-Stokes equation and new solutions of the Stokes equations can be found by superposition of known solutions.

#### 2.2. Basic concepts in electrostatics

Developed by Carl Friedric Guass, Gauss's law gives an equivalence relation between the flux of electric field flowing out of any closed surface and the result of electric charges enclosed within the surface. In a free space, its integral form is [Popović (1971); Stratton (1941)],

$$\oint_{s} \mathbf{E} \cdot d\mathbf{S} = \frac{1}{\epsilon_{0}} \int_{V} \rho dV = \int \nabla \cdot \mathbf{E} dV, \tag{2.3}$$

where  $\rho$  is the density of charges, and  $\epsilon_0$  is the free space permittivity, and **E** denotes the electric field.

Dielectrics are substances that do not possess free electric charges, but can modify an electric field. There are various polarization mechanisms [Morgan & Green (2003)] among which the long-range interfacial polarization is viewed

as playing an important role and it is often referred to as Maxwell-Wagner relaxation mechanism [Jones (1995)]. The polarization vector  $\mathbf{P}$  of the majority of substances is proportional to the total electric field intensity [Popović (1971)]

$$\mathbf{P} = \chi_e \epsilon_0 \mathbf{E} = (\epsilon - \epsilon_0) \mathbf{E}, \tag{2.4}$$

where  $\chi_e$  is referred to as the electric susceptibility and  $\epsilon$  is the dielectric constant, and  $\epsilon = \epsilon_0(1 + \chi_e)$ . The electric displacement vector **D** is defined as [Popović (1971)]

$$\mathbf{D} = \epsilon_0 \mathbf{E} + \mathbf{P} = \epsilon \mathbf{E}. \tag{2.5}$$

Hence the generalized form of Guass Law in dielectrics is [Popović (1971)]

$$\oint_{s} \mathbf{D} \cdot d\mathbf{S} = \int_{V} \rho dV, \quad \text{or} \quad \oint_{s} \mathbf{E} \cdot d\mathbf{S} = \frac{1}{\epsilon} \int_{V} \rho dV. \tag{2.6}$$

When an electric field is applied to a dielectric body, there will be a bulk force exerted on it. On every volume element of the solid body or incompressible fluid, the force density takes the form [Stratton (1941); Morgan & Green (2003)]

$$\mathbf{f} = \rho \mathbf{E} - \frac{1}{2} E^2 \nabla \epsilon. \tag{2.7}$$

From (2.7) and (2.6), we obtain the expression of bulk force exerted on a dielectric fluid [Stratton (1941)]

$$\mathbf{F}_{fluid} = \int_{V} (\epsilon(\nabla \cdot \mathbf{E})\mathbf{E} - \frac{E^{2}}{2}\nabla\varepsilon)dV$$
 (2.8)

Considering a rigid solid body immersed in dielectric medium, by using divergence theorem, the volume integration can be transformed to a surface integration, and the net force exerted by the field on the solid is [Wang *et al.* (1997); Rosales & Lim (2005)]

$$\mathbf{F} = \oint_{\mathbf{s}} [\epsilon \mathbf{E} (\mathbf{E} \cdot \mathbf{n}) - \frac{\epsilon}{2} E^2 \mathbf{n}] dS \tag{2.9}$$

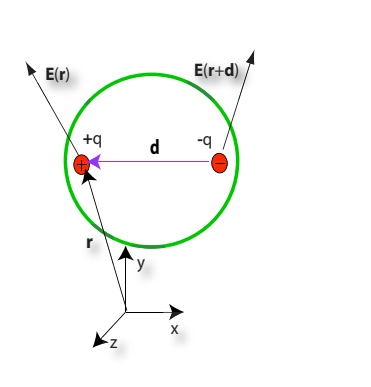
where **n** is the normal vector of the closed surface. This expression is used in calculating the DEP force numerically and theoretically and referred to as MST. It is expected to be the most rigorous method due to its standpoint of classical electrodynamics. However, since no analytic expression for a general electric field is available and the cost of numerical calculation of integration around the surface of many particles is rather high, it is not easy to employ MST to simulate real systems where a large number of particles are manipulated. Calculation of the DEP force of few still rigid particles by MST were performed by Rosales & Lim (2005), and the DEP force acting on a deformable droplet by MST and Level-set methods were calculated by Singh & Aubry (2007).

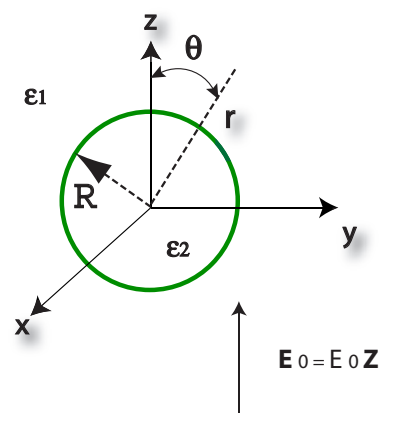
#### 2.3. Effective dipole moment

The effective dipole moment method to calculate electromechanical forces and torques exerted by electric fields on particles is suggested by Jones (1995). It has been popularly used because its simplicity and providing meaningful insights in many important situations [Krupke et al. (2003a); Morgan & Green (2003); Dimaki & Bøggild (2004); Zhang et al. (2005)].

#### 2.3.1. Force on an infinitesimal dipole

The starting point for formulating the force exerted on a dielectric particle is to estimate the net force upon a small physical dipole [Jones 1995], as we know a neutral particle far away can be represented by a dipole moment [Stratton (1941)]. A dipole consists of two charges with opposite sign, -q and +q.





- (a) Schematic of the dipole moment of a particle in an nonuniform electric field
- (b) A dielectric sphere in an parallel uniform electric field

FIGURE 2.1. Derivation of the dipole moment method

In figure 2.1(a), a non-uniform electric field is applied to a dipole with a distance vector **d** between the two charges. The electric field at the two charges are not equal, and the sum of electric forces of the particle is [Jones (1995)]

$$\mathbf{F} = -q\mathbf{E}(\mathbf{r} + \mathbf{d}) + q\mathbf{E}(\mathbf{r}),\tag{2.10}$$

where  $\mathbf{r}$  is the position vector of +q. The electric field at the position of -q can be expressed by Taylor expansion

$$\mathbf{E}(\mathbf{r} + \mathbf{d}) = \mathbf{E}(\mathbf{r}) + \mathbf{d} \cdot \nabla \mathbf{E}(\mathbf{r}) + \dots \tag{2.11}$$

Substituting (2.11) into (2.10), the force is expressed as [Jones (1995)]

$$\mathbf{F} = q\mathbf{d} \cdot \nabla \mathbf{E} + \dots \tag{2.12}$$

If higher order derivatives of the electric field are neglected, and since the dipole moment  $\mathbf{p} = q\mathbf{d}$ , the approximate expression of the force on the dipole can therefore be expressed as [Jones (1995)]

$$\mathbf{F} = \mathbf{p} \cdot \nabla \mathbf{E}.\tag{2.13}$$

#### 2.3.2. Derivation of effective dipole moment

Here we briefly review the derivation of the effective dipole moment method carried out by Jones (1995). Firstly, a homogeneous dielectric sphere of radius R, permittivity  $\epsilon_p$ , and conductivity  $\sigma_p$ , is assumed to be immersed in a dielectric medium of permittivity  $\epsilon_m$  and conductivity  $\sigma_m$ . This system features one interface and one relaxation frequency [Jones (1995)].

The effective dipole moment  $p_{eff}$  of the particle is defined as the moment of an equivalent, free-charge, point dipole that, when immersed in the same dielectric liquid and positioned at the same location as the center of the original particle, produces the same dipolar electrostatic potential [Jones (1995)]. The electrostatic potential  $\phi$  due to a point dipole of moment in a dielectric medium with permittivity  $\epsilon_m$  takes the form [Jones (1995)]

$$\phi(r,\theta) = \frac{qdP_1(\cos\theta)}{4\pi\epsilon_m r^2} + \frac{qd^3P_3(\cos\theta)}{16\pi\epsilon_m r^4} + \dots$$
 (2.14)

where  $P_1$ ,  $P_3$  are Legendre polynomial terms. If only the first term of the right hand side of (2.14) is considered, the approximation of electric field based on the effective dipole moment is written as [Jones (1995)]

$$\phi(r,\theta) = \frac{p_{eff}\cos\theta}{4\pi\epsilon_m r^2},\tag{2.15}$$

where  $\theta$  and  ${\bf r}$  are respectively the polar angle and radial position in spherical coordinates.

The derivation of the effective dipole moment is made under simplifying conditions. That is, the applied electric field outside the particle is taken to be a uniform magnitude  $E_0$  with frequency  $\omega$  and parallel to z axes ( $\mathbf{E}(t) = Re[E_0\mathbf{z}e^{j\omega t}]$ ), see figure 2.1(b). The electrostatic potential satisfies Laplace equation everywhere, and the solutions outside,  $\phi_1(\mathbf{r}, \theta)$ , and inside,  $\phi_2(\mathbf{r}, \theta)$ , are [Jones (1995)]

$$\phi_1(r,\theta) = -Er\cos\theta + \frac{A\cos\theta}{r^2}, \quad r > R$$
 (2.16)

$$\phi_2(r,\theta) = -Br\cos\theta, \quad r < R. \tag{2.17}$$

A and B are unknown coefficients to be determined by the boundary conditions. The first term in the right hand side of (2.16) is the imposed electric field, and the second term is due to the dipole moment of the particle. There are two boundary conditions at the surface r = R. One is that the electric potential

should be continuous, i.e. [Jones (1995); Popović (1971); Stratton (1941)]

$$\phi_1(r = R, \theta) = \phi_2(r = R, \theta).$$
 (2.18)

The other is the conservation law of current flux, which takes the form [Jones (1995)]

$$J_{r1} - J_{r2} + \frac{\partial \sigma_f}{\partial t} = 0, \quad r = R,$$

where  $J_{r1} = \sigma_m E_{r1}$  and  $J_{r2} = \sigma_p E_{r2}$  are the normal components of the ohmic current outside and inside the sphere and  $\sigma_f$  is the free electric surface charge, which can be expressed as [Jones (1995)]

$$\sigma_f = \epsilon_m E_{r1} - \epsilon_p E_{r2}. \tag{2.19}$$

Solving those boundary conditions, A is determined as [Jones (1995)]

$$A = \frac{\epsilon_p^* - \epsilon_m^*}{\epsilon_p^* + 2\epsilon_m^*} R^3 E_0, \tag{2.20}$$

where  $\epsilon^* = \epsilon - j\frac{\sigma}{\omega}$ , and  $j = \sqrt{-1}$ . From (2.15) we know [Jones (1995)]

$$p_{eff} = 4\pi\epsilon_m A. (2.21)$$

#### 2.3.3. DEP force acting on particles in a nonuniform AC field

The general expression for electric field of an AC field can be written as [Morgan & Green (2003); Jones (1995)],

$$\mathbf{E} = Re[\tilde{\mathbf{E}}(\mathbf{x})e^{i\omega t}],\tag{2.22}$$

where the vector  $\tilde{\mathbf{E}}$  is the corresponding complex phasor. Without loss of generality, assuming that the AC electric field has a constant phase across the system, then  $\tilde{\mathbf{E}}$  is real. A general expression for the complex effective moment  $\mathbf{p}_{eff}$  for a dielectric sphere with loss in an electric field takes the form [Jones (1995)]

$$\mathbf{p}_{eff} = 4\pi\epsilon_m Re[K]R^3 \mathbf{E},\tag{2.23}$$

where K is the Clausius-Mossotti factor which is given by [Jones (1995)]

$$K = \frac{\epsilon_p^*(\omega) - \epsilon_m^*(\omega)}{\epsilon_p^*(\omega) + 2\epsilon_m^*(\omega)}.$$
 (2.24)

It can also be expressed by using the Maxwell-Wagner surface polarization relaxation time  $\tau_{MW}$  [Jones (1995)]

$$K(\omega) = K_{\infty} + \frac{K_0 - K_{\infty}}{j\omega\tau_{MW} + 1},$$
(2.25)

where  $\tau_{MW}=rac{\epsilon_p+2\epsilon_m}{\sigma_p+2\sigma_m}$ . Therefore, the low- and high-frequency limits of K are [Jones (1995)]

$$K_{\infty} = \frac{\epsilon_p - \epsilon_m}{\epsilon_p + 2\epsilon_m} \tag{2.26}$$

$$K_{\infty} = \frac{\epsilon_p - \epsilon_m}{\epsilon_p + 2\epsilon_m}$$

$$K_0 = \frac{\sigma_p - \sigma_m}{\sigma_p + 2\sigma_m}.$$
(2.26)

Therefore, the time-average force acting on the particle is expressed as [Morgan & Green (2003); Jones (1995)]

$$\langle \mathbf{F}_{DEP} \rangle = \mathbf{p}_{eff} \cdot \nabla \mathbf{E} = 2\pi R^3 \epsilon_m \beta \tilde{\mathbf{E}} \cdot \nabla \tilde{\mathbf{E}}.$$
 (2.28)

Using the vector identity,  $\nabla (\mathbf{A} \cdot \mathbf{B}) = (\mathbf{A} \cdot \nabla) \mathbf{B} + (\mathbf{B} \cdot \nabla) \mathbf{A} + \mathbf{B} \times (\nabla \times \mathbf{A}) +$  $\mathbf{A} \times (\nabla \times \mathbf{B})$ , and  $\nabla \times \mathbf{E} = 0$  (**E** is an irrational field), (2.28) becomes [Morgan & Green (2003)]

$$\langle \mathbf{F}_{DEP} \rangle = \pi R^3 \epsilon_m \beta \nabla (\tilde{\mathbf{E}} \cdot \tilde{\mathbf{E}}) = \pi R^3 \epsilon_m \beta \nabla |\tilde{\mathbf{E}}|^2.$$
 (2.29)

Considering a homogenous dielectric ellipsoid in a parallel electric field, with the external applied field  $\mathbf{E}_0$  oriented arbitrarily with respect to the ellipsoid and with the components  $E_x$ ,  $E_y$  and  $E_z$  along the semi-axes of the ellipsoid, the x component can be calculated by [Jones (1995)]

$$(\mathbf{P}_{eff})_x = \frac{4\pi abc}{3} \epsilon_m Re \left[ \frac{\epsilon_p^* - \epsilon_m^*}{\epsilon_p^* + (\epsilon_m^* - \epsilon_p^*) L_x} \right] E_x. \tag{2.30}$$

Here the depolarization factor  $L_x$  is defined by [Jones (1995); Rosales & Lim (2005); Stratton (1941)]

$$L_x = \frac{abc}{2} \int_0^\infty \frac{ds}{(s+a^2)R_s},\tag{2.31}$$

where  $R_s = \sqrt{(s+a^2)(s+b^2)(s+c^2)}$ . The y, z components of effective dipole moment can be similarly calculated. Particularly, for a highly elongated prolate ellipsoid (a >> b = c),  $L_{\parallel} \cong 0$  and  $L_{\perp} \cong 1/2$  [Jones (1995)].

The DEP force acting on an ellipsoid can therefore be calculated by [Morgan & Green (2003)]

$$\mathbf{F}_{DEP} = \mathbf{p}_{eff} \cdot \nabla \mathbf{E} = 4\pi abc \epsilon_m Re[K_i] \mathbf{E}_i \cdot \nabla \mathbf{E}, \quad i = x, y, z,$$
 (2.32)

where 
$$K_i = Re\left[\frac{\epsilon_p^* - \epsilon_m^*}{3(\epsilon_p^* + (\epsilon_m^* - \epsilon_p^*)L_i)}\right]$$
  $i = x, y, z$ .

#### 2.3.4. Model of DEP of concentrically layered ellipsoids

Some non-spheral bio-particles can be modeled as concentrically layered dielectric ellipsoids. Asami & Koizumi (1980) presented a model of E.coli bacteria as an ellipsoid covered with two confocal shells corresponding to the membrane and cell wall as shown in Figure 2.2.

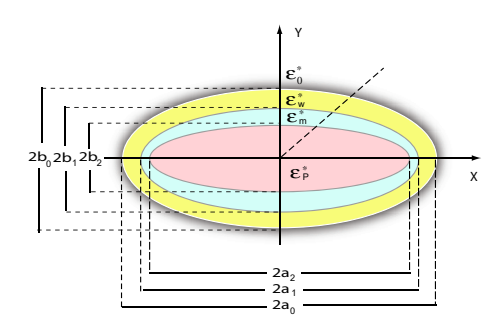


Figure 2.2. Cross section of an electrical cell model represented by three confocal ellipsoids in the x-y

This model gives a corresponding Clausius-Mossotti factor such that the expression for the DEP force can be employed. The details of the derivation are ignored here, and the result is [Asami & Koizumi (1980)]

$$K_n = \frac{1}{3} \frac{\epsilon_{1,n}^* - \epsilon_m^*}{\epsilon_m^* + (\epsilon_{1,n}^* - \epsilon_m^*) A_n}, \quad n = x, y, z,$$
 (2.33)

$$\epsilon_{1,n}^{*} = \epsilon_{w}^{*} \frac{\epsilon_{w}^{*} + (\epsilon_{2,n}^{*} - \epsilon_{w}^{*}) A_{n} + \lambda_{1} (\epsilon_{2,n}^{*} - \epsilon_{w}^{*}) (1 - A_{n})}{\epsilon_{w}^{*} + (\epsilon_{2,n}^{*} - \epsilon_{w}^{*}) A_{n} - \lambda_{1} (\epsilon_{2,n}^{*} - \epsilon_{w}^{*}) A_{n}},$$
 (2.34)

$$\epsilon_{2,n}^{*} = \epsilon_{m}^{*} \frac{\epsilon_{m} * + (\epsilon_{p,n}^{*} - \epsilon_{m}^{*}) A_{n} + \lambda_{2} (\epsilon_{1,k}^{*} - \epsilon_{w}^{*}) (1 - A_{n})}{\epsilon_{m}^{*} + (\epsilon_{p,k}^{*} - \epsilon_{m}^{*}) A_{n} - \lambda_{2} (\epsilon_{p,k}^{*} - \epsilon_{m}^{*}) A_{n}}, \quad (2.35)$$

where

$$\lambda_1 = \frac{(a_0 - d_w)(b_0 - d_w)^2}{a_0 b_0^2}, \qquad (2.36)$$

$$\lambda_2 = \frac{(a_0 - d_w - d_m)(b_0 - d_w - d_m)^2}{(a_0 - d_w)(b_0 - d_w)^2}, \qquad (2.37)$$

$$\lambda_2 = \frac{(a_0 - d_w - d_m)(b_0 - d_w - d_m)^2}{(a_0 - d_w)(b_0 - d_w)^2}, \tag{2.37}$$

and

$$A_x = -\frac{1}{q^2 - 1} + \frac{q}{(q^2 - 1)^{3/2} ln(q + (q^2 - 1)^{1/2})},$$
 (2.38)

$$A_y = A_z = \frac{1}{2}(1 - A_x),$$
 (2.39)

$$q = \frac{a_0}{b_0}. (2.40)$$

Here  $d_w$  and  $d_m$  are supposed to be the thickness of the cell wall and membrane respectively, other parameters used are indicated in Figure 2.2. Substituting (2.33) into (2.32), the DEP force can be calculated.

#### 2.4. Basic molecular dynamics simulation

Molecular dynamics (MD) simulation is based on the ergodic hypothesis, a fundamental axiom of statistical mechanics, which states that the time average equals the ensemble average [Allen & Tildeslley (1987); Sadus (1999)]

$$\langle A \rangle_{ensemble} = \langle A \rangle_{time}$$
 (2.41)

The essence of MD simulation is to numerically solve step-by-step the classical equations of motion

$$m_i \ddot{\mathbf{r}} = \mathbf{f}_i, \quad \mathbf{f}_i = -\frac{\partial U}{\partial \mathbf{r}_i}$$

where  $m_i$  is the mass of *i* particle,  $\mathbf{f}_i$  is the force acting on it and  $\mathbf{r}$  is its coordinator. A general form of empirical potential function in chemistry takes the form as [Refson (2001)]

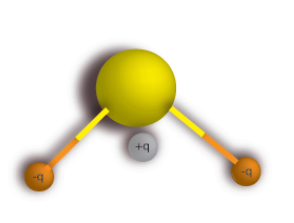
$$U(\mathbf{r}) = \sum_{bonds} k_i^b (r_i - r_0)^2 + \sum_{angles} k_i^a (\theta_i - \theta_0)^2 + \sum_{dihe} k_i^d [1 + \cos(n_i \theta_i + \delta_i)] + \sum_i \sum_{j \neq i} 4\varepsilon_{ij} [(\frac{\sigma_{ij}}{r_{ij}})^{12} - (\frac{\sigma_{ij}}{r_{ij}})^6] + \sum_i \sum_{j \neq i} \frac{q_i q_j}{4\pi\epsilon_0 r_{ij}}.$$
 (2.42)

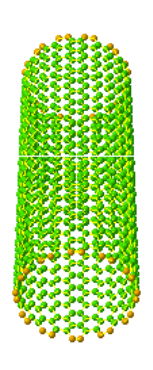
In the right hand side of (2.42), the first three terms are so-called bond potentials, and the last two terms are non-bond potentials [Allen (2004)]. The term  $U_{bond}$  models the oscillations about the equilibrium bond,  $U_{angles}$  models the oscillations of three atoms about an equilibrium angle, and  $U_{dihe}$  models the torsional rotation of 4 atoms about a central bond. The non-bond potentials are Lennard-Jones potential modeling van del Waals force and Coulomb potential related to electrostatic force. With a rigid O-H bond length and fixed angle between two H-O bonds, the commonly used extended simple point charge (SPC/E) model of water molecule therefore contains only non-bond potentials [Berendsen et al. (1987); Todorov & Smith (2006)]. To investigate the oscillations and vibrations inside molecules, flexible models have to be used, i.e., bond potential should be included [Marti & Gordillo (2002); Gordillo & Marti (2002)].

Chemistry force fields commonly are unable to model the process of chemical bond breaking and reactions explicitly because they employ preset bonding arrangement. On the other hand, many of the potentials used in physics can describe several different coordination systems and bond breaking. For example, Brenner potential for hydrocarbon and carbon nanotube is one of the bond order potentials, which take the form [Brenner (1990); Albe *et al.* (2002)]

$$V_{ij}(r_{ij}) = V_{repulsive}(r_{ij}) + b_{ijk}V_{attractive}(r_{ij}).$$
(2.43)

We can see that Brenner potential consists of simple pair potentials depending on the distance between two atoms  $r_{ij}$ , and the strength of attractive potentials is modified by the environment of the atoms i and j (number of bonds





(a) Schematic of a water molecule model.

(b) Schematic of of a singlewalled carbon nanotube.

FIGURE 2.3. Schematics of water molecule and SWNT

and possibly also angles between bonds and distances from other atoms) via the  $b_{ijk}$  term. Carbon nanotubes are important materials in many applications of nanotechnology [Saito  $et\ al.\ (1998)$ ], electronics, optics and other fields and are categorized as single-walled nanotubes (SWNTs) and multi-walled nanotubes (MWNTs). Due to their unique electric properties, SWNTs are the most likely candidates for miniaturizing electronics beyond the micro electromechanical scale, which is currently the basis of modern electronics. A SWNT can be viewed as a seamless cylinder which is obtained by wrapping a one-atom-thick graphite sheet. The way it is wrapped can be represented as a pair of indices (n,m), which is called the chiral vector. SWNTs with different (n,m) can possess dramatically different physical properties, and a thorough description can be found in the book of Saito  $et\ al.\ (1998)$ . Briefly speaking, SWNTs are classified as metallic SWNTs and semiconducting SWNTs due to their entire different electric properties. Figure 2.3(b) shows an armchair SWNT (when n=m).

The thermodynamic state of a system is usually defined by a small set of parameters (i.e., number of particle N, the temperature T, the pressure P and the volume V). Other thermodynamic properties (e.g., density  $\rho$ , chemical potential  $\mu$ , heat capacity  $C_v$  etc.) can be derived from the results of MD simulations [Allen & Tildeslley (1987); Sadus (1999)].

There are four common classes of statistical ensembles in MD simulation: microcanonical, canonial, grand canonial and isothermal-isobaric due to which set of parameters is chosen [Allen & Tildeslley (1987)]. In equilibrium states, all ensembles are equivalent. The choice is entirely a matter of convenience [Sadus (1999)].

The ensemble we employ is the canonial ensemble, in which the constraints are V, N and T. To initialize a canonial ensemble, temperature control needs to be taken for some time steps in the beginning to equilibrate the system. The reason is that the preset position of molecules usually possesses high potential energy which need to be taken away after it is transformed to kinetic energy by applying Newtons second law. The simplest method is velocity scaling as described here [Sadus (1999)].

The kinetic energy per particle for the ensemble can be calculated from  $\langle K \rangle = \frac{1}{2N} \langle \sum_{i}^{N} m_{i} \mathbf{v}_{i} \cdot \mathbf{v}_{i} \rangle$ , and from the kinetic theory of gases, we know  $\langle K \rangle = \frac{3}{2}kT$ . Equating the right hand side of these two formulas, we obtain the following expression to calculate temperature

$$T_A = \frac{1}{3Nk} < \sum_{i=1}^{N} m_i \mathbf{v}_i \cdot \mathbf{v}_i > . \tag{2.44}$$

Expression (2.44) enables us to determine the actual temperature  $(T_A)$  for the ensemble at any time. Consequently, the velocities can be scaled with respect to the actual and desired temperatures  $(T_D)$  as [Sadus (1999)]

$$\mathbf{v}^{new} = \mathbf{v} \sqrt{\frac{T_D}{T_A}}. \tag{2.45}$$

The time integration method employed is the velocity Verlet algorithm, which gives a global error as  $O(\Delta t^2)$  and offer greater stability than the much simpler Euler Forward method whose error is  $O(\Delta t)$ . The algorithm takes the forms as [Allen & Tildeslley (1987)],

$$\mathbf{r}(t+\delta t) = \mathbf{r}(t) + \delta t \mathbf{v}(t) + \frac{1}{2} \delta t^2 \mathbf{a}(t),$$

$$\mathbf{v}(t+\delta t) = \mathbf{v}(t) + \frac{1}{2} \delta t [\mathbf{a}(t) + \mathbf{a}(t+\delta t)].$$
(2.46)

The orientation of a rigid molecule can be specified by three independent Euler angles which determining the rotation transform matrix. However a serious drawback of this method is that a singular equation of motion may cause awkward numerical properties. An elegant and effective solution which has been popularly employed is the use of the generalized coordinates – quaternions. The detailed description of quaternion can be found in many sources [Shoemake (1985); Allen & Tildeslley (1987)].

The static dielectric constant of isotropic bulk water can be calculated by [Marti et al. (1994)]

$$\epsilon_0 = 1 + \frac{4\pi}{3Vk_BT}\phi^c(0),$$
(2.47)

where  $k_B$  is the Boltzman constant and  $\phi^c$  is the collective time correlation function of dipole moments, which is calculated by

$$\phi^c(t) = \langle \mathbf{M}(t) \cdot \mathbf{M}(0) \rangle, \tag{2.48}$$

where 
$$\mathbf{M}(t) = \sum_{i=1}^{N} \mu_i(t)$$
, and  $\mu_i(t) = \sum_{j=1}^{ns} q_j \cdot \mathbf{d}_j$  is the dipole moment of the i-

molecule. Dipole moments are usually measured in units named debye (debye unit D:  $1D = 3.336 \times 10^{30} \text{C/m}$ ) in the honor of Dutch physicist Peter Debye. Although the dipole moment of an isolated water monomer is around 1.85 Debye, in the liquid phase it increases to the value from 2.4 to 2.6 D due to the polarization by the environment [Gregory et al. (1997)]. Simulations of liquid water by pair potential generally require the dipole moment of water molecules located in 2.3 to 2.4 to reproduce experimental data [Laasonen et al. (1993)]. The SPC/E model therefore gives a permanent dipole moment value of water molecules as 2.35 D [Berendsen et al. (1987); English & Macelroy (2002)].

#### CHAPTER 3

# Modeling and numerical treatment

This chapter describes numerical models for calculating the force of particles experience in DEP separation, and numerical treatment implemented in molecular dynamics (MD) study of dielectric property of water inside SWNT.

#### 3.1. Particle dynamics method

In this section, particle dynamics model provides a way of solving the equations of the motion of each particle by replacing them with a set of finite difference equations which are solved on a step-by-step basis.

We view the particles as spheres with size much smaller than the length scale of the electrodes. Under such assumption, we do not consider the rotational motion of particles. On the micro level, we consider the flow to be Stokes flow. There will be no need to solve the Navier-Stokes equations either. The reason is that according to the specified micro-scale condition, the analytical expression for the hydrodynamic forces between suspended particles in Stokes flows has been well established. Those functions could be directly adopted to account for the hydrodynamic interaction between particles. Besides, since we assume the particles to be spherical and without deformation, it is reasonable to simply add repelling forces which become significant when two particles come to touch each other. The net DEP forces acting on the particles by the field and the interactive electrostatic forces from other particles are added on the centers of mass of the particle. Therefore, we are able to include all the important forces into a set of coupled equations of motion (ordinary differential equations) for many-body systems.

#### 3.1.1. Terminal speed of particle in micro and nano fluid

For simplification, we consider a sphere in a fluid flow with speed  ${\bf v}$  experiencing an external force  ${\bf F}$ . According to the Newton Second Law

$$m\frac{d\mathbf{u}}{dt} = \mathbf{F} - 6\pi\mu a(\mathbf{u} - \mathbf{v}). \tag{3.1}$$

The second term of (3.1) is the *Stokes drag* force acting on the particle from the fluid [Morgan & Green (2003)].  $\mathbf{u}$ , m,  $\mu$  and a are the speed of particle, the mass of the sphere , the viscosity of fluid and the radius of the sphere respectively.

The solution of (3.1) is easy to obtain. When the initial particle velocity is zero, it can take the form [Morgan & Green (2003)]

$$\mathbf{u} = \left(\frac{\mathbf{F}}{6\pi\mu a} + \mathbf{v}\right)\left(1 - e^{\frac{6\pi\mu a}{m}t}\right). \tag{3.2}$$

It is natural to take the characteristic time as  $\tau = \frac{m}{6\pi\mu a} = \frac{2\rho a^2}{9\mu}$ . If the density of the particle,  $\rho$ , is taken as the same as water, the radius of the particle  $a\approx 10^{-6}$  m and the fluid viscosity is taken as water, then  $\tau\approx 10^{-6}$  s. Since the limit of time for observation is about 1/30 s, which is much longer than  $\tau$  [Morgan & Green (2003)], therefore the particle that is observed moves at the terminal speed. For particles of nanoscale, the characteristic time  $\tau$  is even smaller. This means that in microsystems, the inertial effect is negligible and the terminal speed of the particle takes the form

$$\mathbf{u}_t = \frac{\mathbf{F}}{6\pi\mu a} + \mathbf{v} \tag{3.3}$$

#### 3.1.2. Hydrodynamic interaction

In this model, the hydrodynamic force is considered by the following way. In micro and nano flows where the Reynolds number  $Re \ll 1$  and in a steady state, the nonlinear terms and time derivatives can be neglected from the equation (2.2). By further assuming that external forces are absent, the governing equations become

$$\nabla^2 \mathbf{U} = \nabla p, \tag{3.4}$$

$$\nabla \cdot \mathbf{U} = 0, \tag{3.5}$$

which are known as the Stokes or Creeping flow equations. The motion of a given particle induces a flow field in the solvent, which will be felt by every other particle. Consequently, these particles experience a force resulting from the hydrodynamic interaction with the original particle. By solving the Stokes equation for a two-particle case, the first order expression for the mobility tensor is, as given by Oseen [Elimelech et al. (1995)]

$$\mu_{ij} = \delta_{ij} \frac{1}{6\pi\mu a} + (1 - \delta_{ij}) \frac{1}{8\pi\mu r_{i,j}} \left( \mathbf{1} + \frac{\mathbf{r}_{ij}\mathbf{r}_{ij}}{r_{ij}^2} \right), \tag{3.6}$$

where **1** is the unit tensor,  $\mathbf{r}_{ij} = \mathbf{r}_i - \mathbf{r}_j$ ,  $r_{ij} = |\mathbf{r}_i - \mathbf{r}_j|$ , a is the radius of the particle, and  $\delta_{ij}$  is the Kronecker delta. At last, we get the velocity expression as

$$\mathbf{U}_i = -\sum_{j=1}^N \mu_{ij} \cdot \mathbf{F}_j \tag{3.7}$$

Corrections resulting from more than three-body interactions  $(n \ge 3)$  are not taken into account. The concept of three-body interaction is, particle A

can affect particle C directly and affect C indirectly by directly affect particle B. The indirect influences are expressed by correction functions of the order  $(\frac{a}{r_{ij}})^2$  or higher. The two-body hydrodynamic force acting on particle i can be expressed as [Elimelech *et al.* (1995)]

$$\mathbf{F}_{drag,i} = -\sum_{j=1}^{N} \zeta_{ij} \cdot \mathbf{U}_{j}, \tag{3.8}$$

where tensor  $\zeta_{ij}$  is defined as [Elimelech *et al.* (1995)]

$$\zeta_{ij} = \delta_{ij} (6\pi\mu a) + (1 - \delta_{ij}) 6\pi\mu a \frac{3a}{4r_{ij}} (1 + \frac{\mathbf{r}_{ij}\mathbf{r}_{ij}}{r_{ij}^2}). \tag{3.9}$$

#### 3.1.3. Electrostatic interaction

For an isolated spherical particle suspended in an electric field **E**, the effective dipole moment is given by [Morgan & Green (2003); Kadaksham *et al.* (2004)]

$$\mathbf{p} = 4\pi\epsilon_m \beta a^3 \mathbf{E},\tag{3.10}$$

where  $\beta$  is the real part of Causius-Mossotti factor and a is the radius of the particle. The interaction forces between particle i and j are based on the dipole moment of these particles, which take the forms

$$\mathbf{p}_i = 4\pi \epsilon_m \beta a^3 \mathbf{E}_i, \quad \mathbf{p}_j = 4\pi \epsilon_m \beta a^3 \mathbf{E}_j, \tag{3.11}$$

where  $\mathbf{E}_i$  and  $\mathbf{E}_j$  are electric field vector at the positions of centers of particle i and j respectively. Written in the vector form, the expression of electrostatic interactions  $\mathbf{F}_{D,ij}$  is expressed as [Kadaksham *et al.* (2004)]

$$\mathbf{F}_{D,ij} = \frac{1}{4\pi\epsilon_m} \frac{3}{r^5} (\mathbf{r}_{ij}(\mathbf{p}_i \cdot \mathbf{p}_j) + (\mathbf{r}_{ij} \cdot \mathbf{p}_i)\mathbf{p}_j + (\mathbf{r}_{ij} \cdot \mathbf{p}_j)\mathbf{p}_i - \frac{5}{r^2} \mathbf{r}_{ij}(\mathbf{p}_i \cdot \mathbf{r}_{ij})(\mathbf{p}_j \cdot \mathbf{r}_{ij})). \tag{3.12}$$

As we already discussed, the inertial effect is negligible in micro systems. Therefore, for particle i, the total force is zero, i.e.,

$$\mathbf{F}_{dep,i} + \mathbf{F}_{dip,i} + \mathbf{F}_{wall,i} + \mathbf{F}_{p,i} + F_{drag,i} = 0, \tag{3.13}$$

where  $\mathbf{F}_{dep,i}$  is the DEP force,  $\mathbf{F}_{dip,i} = \sum_{j=1,j\neq i}^{N} \mathbf{F}_{D,ij}$  is the sum of the inter

particle electrostatic forces acting on i particle, and  $\mathbf{F}_{wall,i}$  is the repulsive force from the wall, and  $\mathbf{F}_{p,i}$  is the sum of repulsive forces from other particles. Substituting (3.8) into (3.13), we obtain the final system of equations to solve.

After non-dimensionalization, the system of equations takes the form

$$\frac{d\mathbf{x}_{i}}{dt} = P_{1} \sum_{j=1, j \neq i}^{N} \mathbf{F} \mathbf{G}_{i, j} \cdot \frac{d\mathbf{x}_{j}}{dt} + P_{2} \mathbf{F} \mathbf{D}_{i} + P_{3} \sum_{j=1, j \neq i}^{N} \mathbf{F} \mathbf{D} \mathbf{I} \mathbf{P}_{ij} + \mathbf{F}_{W, i} + \mathbf{F}_{P, i}$$
(3.14)

with the following definitions:

• Characteristic variables:

L: Length  $V_0$ : Potential T: Time

• Dimensionless parameters:

$$P_1 = \frac{3r}{4L}, \quad P_2 = \frac{2\beta r^2 \epsilon_m V_0^2 T}{3L^4 \mu}, \quad P_3 = \frac{2\epsilon_m \beta^2 r^5 V_0^2 T}{\mu L^7} = 3\beta (\frac{r}{L})^3 P_2$$

• Dimensionless functions

$$\mathbf{F}\mathbf{D}_{i} = \nabla |\mathbf{E}^{*}|^{2},$$

$$\mathbf{F}\mathbf{G}_{ij} = \frac{1}{R_{ij}^{*}}(\mathbf{1} + \hat{\mathbf{R}}_{ij}^{*}\hat{\mathbf{R}}_{ij}^{*}),$$

$$\mathbf{F}\mathbf{D}\mathbf{I}\mathbf{P}_{ij} = \frac{1}{(R_{ij}^{*})^{5}}(\mathbf{R}_{ij}^{*}(\mathbf{p}_{i}^{*}\cdot\mathbf{p}_{j}^{*}) +$$

$$(\mathbf{R}_{ij}^{*}\cdot\mathbf{p}_{i}^{*})\mathbf{p}_{j}^{*} + (\mathbf{R}_{ij}^{*}\cdot\mathbf{p}_{j}^{*})\mathbf{p}_{i}^{*} - \frac{5}{(R_{ij}^{*})^{2}}\mathbf{R}_{ij}^{*}(\mathbf{p}_{i}^{*}\cdot\mathbf{R}_{ij}^{*})(\mathbf{p}_{j}^{*}\cdot\mathbf{R}_{ij}^{*})), (3.15)$$

where  $\mathbf{FG_i}$  is the dimensionless form of hydrodynamic force (see expression 3.8),  $\mathbf{FD_i}$  is the dimensionless form of DEP force (see expression 2.29), and  $\mathbf{FDIP_{ij}}$  is the dimensionless form of  $\mathbf{F}_{D,ij}$ . Here  $\mathbf{F}_{W,i}$  and  $\mathbf{F}_{P,i}$  denote dimensionless repulsive force from wall and other particles respectively. All the variables with star symbol as upper index are the nondimensionless forms of those variables without index, and  $\hat{\mathbf{R}}_{ij} = \frac{\mathbf{r}_{ij}}{r_{ij}}$ . By comparing the dimensionless parameters  $P_1, P_2, P_3$ , the relative magnitudes between those forces can be determined.

#### 3.1.4. Superposition of DEP forces

A simplified particle dynamical model (ignoring the interactive forces between particles) is applied in the calculation for enhancing the trapping efficiency of *E.coli* bacteria. In this problem, the Clausius-Mossotti factor is a frequency-dependent complex number with the real part value between -0.5 and 1. We expect that if proper superimposed electric fields (with different frequencies) are used in the calculation, the trapping efficiency can be enhanced greatly. Below is the simple mathematical proof of the validity of the superposition of DEP forces.

Since  $\mathbf{E} = \nabla \tilde{\phi}$  ( $\tilde{\phi}$  is the potential of electric field which can be written as  $\tilde{\phi} = \phi \sin \omega t$  with  $\phi$  only depending on space), after nondimensionlization, we get the relationship between  $\mathbf{F}_{dep}$  and potential  $\phi$  as:

$$\mathbf{F}_{dep} = \nabla(\nabla\phi\sin(\omega t))^2. \tag{3.16}$$

The time average force is then

$$\langle \mathbf{F} \rangle = \frac{1}{T} \nabla (\nabla \phi)^2 \int_0^T \sin^2(\omega t)$$
 (3.17)

$$= \frac{1}{2}\nabla(\nabla\phi)^2. \tag{3.18}$$

Assuming two harmonic potentials with different frequencies are introduced at the same time to a system, we have the superimposed electric potential as

$$\tilde{\phi}_{total} = \phi_1 \sin(\omega_1 t) + \phi_2 \sin(\omega_2 t). \tag{3.19}$$

Thus, we get

$$(\nabla \tilde{\phi}_{total})^2 = (\nabla \phi_1 \sin(\omega_1 t) + \nabla \phi_2(\omega_2 t))^2,$$

$$= \nabla \phi_1^2 \sin^2(\omega_1 t) + \nabla \phi_2^2 \sin^2(\omega_2 t) + 2\nabla (\phi_1 \sin(\omega_1 t) \nabla \phi_2 \sin(\omega_2 t).$$
(3.20)

The time-average force is

$$\langle \mathbf{F} \rangle_{total} = \frac{1}{T} \int_{0}^{T} F_{dep} dt,$$

$$= \frac{1}{T} \nabla (\nabla \phi_{1})^{2} \int_{0}^{T} \sin^{2}(\omega_{1}t) dt + \frac{1}{T} \nabla (\nabla \phi_{2})^{2} \int_{0}^{T} \sin^{2}(\omega_{2}t) dt$$

$$+ 2 \frac{1}{T} \nabla (\nabla \phi_{1} \nabla \phi_{2}) \int_{0}^{T} \sin(\omega_{1}t) \sin(\omega_{2}t) dt. \tag{3.21}$$

When T tends to infinity, it is easy to verify that the last term of (3.21) tends to zero, and (3.21) becomes:

$$<\mathbf{F}>_{total} = \frac{1}{2}\nabla(\nabla\phi_1)^2 + \frac{1}{2}\nabla(\nabla\phi_2)^2 = <\mathbf{F}>_1 + <\mathbf{F}>_2.$$
 (3.22)

Therefore, it is correct to superimpose the DEP forces corresponding to superimposed AC fields of different frequencies.

#### 3.2. Fluid dynamics in micro and nano systems

Experimental results [Müller et al. (1996); Ramos et al. (1998); Green et al. (2002); Morgan & Green (2003)] have shown that in DEP systems with microelectrodes, AC electric fields can generate local fluid motion. Two types of electric field-driven fluid motion occurs when the fields are large and the scale of the system is small.

The first type of fluid flow is caused by the bulk force acting on the dielectric fluid under an applied electric field [refer to expression (2.7)]. The gradient of

electric permittivity  $\epsilon$  is caused by temperature gradient due to the extremely high gradient of electric field. In an AC electric field, it takes the form [Ramos et al. (1998); Morgan & Green (2003); Castellanos et al. (2003); Feldman et al. (2007)]

$$\langle f_{\mathbf{E}} \rangle = -\frac{1}{2} \left[ \left( \frac{\nabla \sigma}{\sigma} - \frac{\nabla \epsilon}{\epsilon} \right) \cdot \mathbf{E}_0 \frac{\epsilon \mathbf{E}_0}{1 + (\omega \tau)^2} + \frac{1}{2} |E_0|^2 \nabla \epsilon \right],$$
 (3.23)

where

$$\nabla \sigma = \frac{d\sigma}{dT}(\nabla T), \quad \nabla \epsilon = \frac{d\epsilon}{dT}(\nabla T), \quad \nabla^2 T = \sigma |\mathbf{E}|^2.$$
 (3.24)

Essentially caused by joule heating, this flow is therefore often referred to as the electrothermal flow. Although there is no analytic solution for general systems with arbitrary geometries, numerical calculation of flow can be easily obtained. For example, by using finite element method, we are able to solve the Navier Stokes equations coupled with the external electrothermal force.

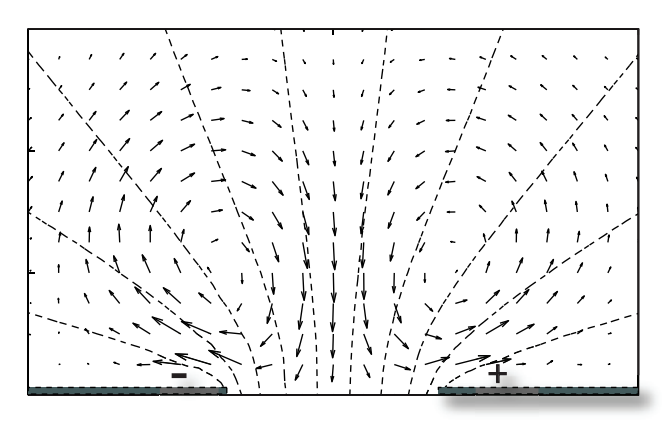


FIGURE 3.1. Schematic of electrothermal flow. The dash lines are isolines of electric potential.

Figure 3.1 shows the electric potential lines and the resulting fluid motion in a DC electric field. The electrothermal flow therefore is corresponded to the equation (3.23) when frequency is zero. We should keep in mind that the electrothermal flow pattern can be entirely different in high frequency. This geometry has been extensively used [Morgan & Green (2003); Krupke *et al.* (2003a)] where a pair of long electrodes is placed in parallel with infinity length, and these systems can therefore be regarded as 2D problems.

The other kind of fluid flow is often referred to as AC electroosmosis, which is related to the charging of the double layer on the surface of microelectrodes. Detailed illustration can be found in the works of Ramos *et al.* (1998), Morgan & Green (2003) and Castellanos *et al.* (2003). Here we present the final form

of the time-averaged fluid velocity along the surface of electrode

$$\langle u_x \rangle = \frac{1}{8} \frac{\varepsilon \kappa \phi_0}{\mu x (1 + \Omega^2)^2}, \tag{3.25}$$

where  $\phi_0$  is the applied voltage, and  $\Omega = (12)\pi\kappa x(\epsilon/\sigma)\omega$ ,  $\kappa^{-1}$  is the Debye width of the electric double layer. Since the typical  $\kappa^{-1}$  for the EDL is several nm [Morgan & Green (2003)], taking  $\kappa^{-1} = 1$  nm, an estimation of AC electroosmosis corresponding to a system of separating SWNT is calculated and plotted in Figure 3.2

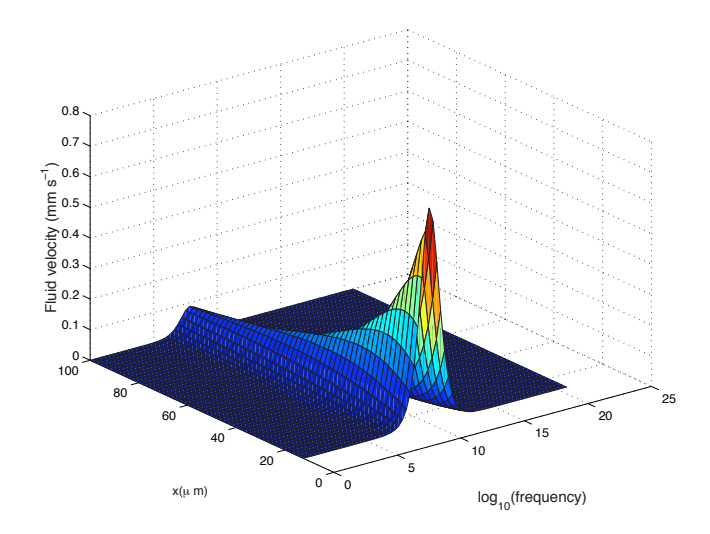


FIGURE 3.2. AC electroosmotic fluid flow at the surface of an electrode. The solution is 1% SDBS, and the data is calculated as a function of frequency of the applied electric field, and the distance from the edge of the electrode. The potential voltage applied is 20 Volt, and the gap between electrode is 20  $\mu$ m.

Understanding the electrokinetic motion of fluid is of great importance in particle separation and manipulation in micro and nano systems. Since both fluid flows are frequency-dependent, Morgan & Green (2003) summarized the frequency ranges where each of the two electric field-driven fluid flows dominates. In brief, at low frequency ( $f < 100~{\rm kHz}$ ), the dominant fluid flow is AC electroosmosis, and at higher frequency, electrothermal fluid flow dominates.

#### 3.3. Modeling of DEP based on distributed charge density

DEP is used to manipulate highly elongated particles, i.g., SWNTs [Krupke et al. (2003a); Zhang et al. (2005)], rod-shape virus [Green et al. (1997)], and

rod-like DNA [Tuukkanen et al. (2007)] which are natural to be regarded as rigid fibers. Despite the fact that the effective dipole moment method is generally used to calculate the DEP force of those particles [Krupke et al. (2004); Zhang et al. (2006)], it is not so accurate since the length of the particles is comparable to the characteristic length of the system (the width of the gap between electrodes).

Considering a rigid fiber, slender body theory is often used in fluid mechanics and electrostatics. Its essential idea is to take advantage of the slenderness of a body to obtain an approximation to a field surrounding it and the net effect of the field on the body. The slender body theory in Stokes flow fluid was first developed by Batchelor (1970). While in electrostatics, Geer (1976) derived the asymptotic expression for the induced charge density of slender dielectric body embedded in a specified but arbitrary electrostatic potential field  $\phi$ . More studies about electric field around slender bodies can be found in the papers of Barshinger & Geer (1987) and Sellier (2001). In those works, electric fields were solved by asymptotic expansions with high order accuracy however demanding expensive calculate cost. Therefore, the current model is suggested aiming to provide a practical solution to calculate the disturbed electric fields and furthermore the DEP force acting on a slender body (which is approximated by a prolate ellipsoid). The accuracy is expected to be higher than the effective dipole moment method since it concerns arbitrary number of points along the centerline of the particle while effective dipole moment only utilizes the electric field in the center point.

Figure 3.3 shows a modeled ellipsoid. The shape parameter, slenderness  $\delta = \max(x^2 + y^2)/\mathrm{L}$  should be much less than 1.

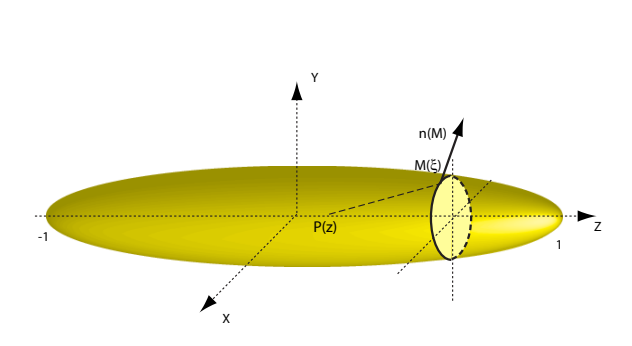


FIGURE 3.3. The schematic of the modeled ellipsoid. The radius R satisfies,  $R = \sqrt{x^2 + y^2} = \delta S(z)$  with  $S(z) = \sqrt{1 - z^2}$ , which leads to R(-1) = R(1) = 0.

The starting point of this model is that when considering an ellipsoid immersed in a dielectric medium, we assume that the induced charges are distributed along the centerline of the particle only depending on the z coordinator. By enforcing the boundary conditions on the interfaces between two dielectrics, we obtain the expression of the induced charge as

$$\sigma(z) = (1 - \frac{1}{\epsilon}) \left[ -\int_{-1}^{1} \frac{\overrightarrow{PM} \cdot \vec{n}}{|PM|^{3}} \sigma(\xi) \delta S(\xi)^{1/2} d\xi + \epsilon_{0} \frac{\partial \phi^{0}(z)}{\partial \vec{n}} \right],$$

where  $\sigma(z)$  is the unknown induced charge density and  $\phi^0(z)$  is the original electric field, and  $\vec{n}$  is the normal vector of the surface of ellipsoid and  $\epsilon$  is the ratio between the dielectric permittivity of the ellipsoid and medium.

Based on the calculated electric charge densities, the resulting electric field can be obtained and also the DEP force of each particle can be calculated. By this means, the interaction between particles due to the induced charge are naturally concerned. For AC electric field, similar expressions can be derived and the only difference is that the dielectric permittivities in expressions are substituted by complex permittivities.

#### 3.4. Ewald summation

To calculate the dielectric property of water by MD simulation, proper periodic boundary treatment should be taken. This is the motivation of the implementation of Ewald summation. Because the electric potential is a long range force  $(\frac{1}{r})$ , compared to Lennard-Jones potential  $(\frac{1}{r^6})$ , a large domain needs to be taken into account. Ewald summation is a technique for efficiently summing the interaction between an ion and all its periodic images [Allen & Tildeslley (1987)] inside a large sphere whose radius is determined by the maximum value of  $\mathbf{n}$ . If in the unit cell there are M charges, the total electric energy (potential) of the system may be written as

$$V = \frac{1}{2} \sum_{\mathbf{n}}' \left( \sum_{i=1}^{M} \sum_{j=1}^{M} q_i q_j |\mathbf{r}_{ij} + \mathbf{n}|^{-1} \right),$$
 (3.26)

where  $q_i$  is the charge of i ion. The prime indicates that we omit i=j for  $\mathbf{n} = 0$ . The charge neutrality condition is

$$\sum_{i=1}^{M} q_i = 0. (3.27)$$

For simplicity of notation, all factors of  $4\pi\epsilon_0$  are omitted. The sum over  $\mathbf{n}$  is the sum over all cubic lattice cells,  $\mathbf{n}=(n_xL,n_uL,n_zL)$ . However, this sum is only conditionally convergent. Ewald summation decomposes the interaction potential into a short-range component summed in real space and a long-range component summed in Fourier space. Its advantage is the rapid convergence of

the Fourier-space summation compared to its real-space equivalent when the real-space interactions are long-range. The final form for a sphere surrounded by a good conductor ( $\epsilon_s = \infty$ ) is [Allen & Tildeslley (1987); Leeuw *et al.* (1980); Heyes (1984)].

$$V(\epsilon_{s} = \infty) = \frac{1}{2} \sum_{i=1}^{M} \sum_{j=1}^{M} \left( \sum_{|\mathbf{n}|=0}^{Nmax'} q_{i}q_{j} \frac{erfc(\kappa|\mathbf{r_{ij}} + \mathbf{n}|)}{\mathbf{r}_{ij} + \mathbf{n}} \right)$$

$$+ \left( \frac{1}{\pi L^{3}} \right) \sum_{\mathbf{k} \neq \mathbf{0}}^{KSQmax} q_{i}q_{j} (4\pi^{2}/k^{2}) exp(-k^{2}/4\kappa^{2}) \cos(\mathbf{k} \cdot \mathbf{r}_{ij}))$$

$$- \left( \kappa/\pi^{1/2} \right) \sum_{i=1}^{N} q_{i}^{2}, \qquad (3.28)$$

where L is the length of the cubic cell. The first term is so-called real space term (the prime means when  $\mathbf{n} = 0$ ,  $j \neq i$ ) denoted by  $V_r$ , the second term is K-space term denoted by  $V_k$ , the third term is so called self-energy term.  $\kappa$  is the parameter to control the decomposition between sum of the real-space and K-space. Here  $\operatorname{erfc}(x)$  is the complementary error function [Allen & Tildeslley (1987)]

$$\operatorname{erfc}(x) = \frac{2}{\sqrt{\pi}} \int_{x}^{\infty} \exp(-t^{2}) dt. \tag{3.29}$$

By taking derivative of the potential ( $\mathbf{f} = -\nabla V$ ), we obtain the expressions to calculate the forces, which take the forms

$$\mathbf{F}^{r}(i) = q_{i} \sum_{j=1}^{M} \sum_{|\mathbf{n}|=0}^{Nmax'} q_{j} \frac{\mathbf{r}_{ij,\mathbf{n}}}{r_{ij,\mathbf{n}}^{3}} \left[ \operatorname{erfc}(\kappa r_{ij,\mathbf{n}}) + \frac{2\kappa}{\sqrt{\pi}} r_{ij,\mathbf{n}} \exp(-(\kappa r_{ij,\mathbf{n}})^{2}) \right],$$

$$\mathbf{F}^{k}(i) = \frac{4\pi}{L^{3}} q_{i} \sum_{j=1}^{M} \sum_{k\neq 0}^{KSQmax} q_{j} \mathbf{k} \frac{1}{k^{2}} \exp(-(\frac{k^{2}}{4\kappa^{2}})) \sin(\mathbf{k} \cdot \mathbf{r}_{ij}), \qquad (3.30)$$

where  $\mathbf{r}_{ij,n} = \mathbf{r}_{ij} + \mathbf{n}$ , and  $r_{ij,n} = |\mathbf{r}_{ij} + \mathbf{n}|$ . The term  $\mathbf{F}^r$  denotes the force in real space, and  $\mathbf{F}^k$  means the force in K-space.

For the dipole systems, there is similar expression as (3.26), except the charges are substituted by dipole moments. However we adopted another method, i.e., expression (3.26) can be employed directly by subtracting the intramolecular energy from it. The intramolecular energy takes the form

$$V^{self} = \sum_{i=1}^{W} \left( \sum_{a=1}^{n_s} \kappa q_{i,a}^2 / \pi^{\frac{1}{2}} + \frac{1}{2} \sum_{a=1}^{n_s} \sum_{b \neq a}^{n_s} q_{i,a} q_{i,b} \frac{1}{d_{ab}} \right), \tag{3.31}$$

where  $n_s$  is the number of atoms in one molecule,  $d_{ab}$  is the distance between atom a and b and d is the number of molecules in the system.

In the actual MD code, three parameters are often used to control the convergence of the sums.

- Nmax, an integer defining the range of the real-space sum and controls its maximum number of vectors
- KSQmax, an integer restricting the summation range in the reciprocalspace and its number of vectors
- $\kappa$ , the Ewald convergence parameter, determining the relative rate of convergence between the real and reciprocal sums

Note that a large  $\kappa$  makes the real-space sum converge fast. Because as  $\kappa \to \infty$ ,  $\operatorname{erfc}(\kappa x) \to 0$ . This means that a small number of  $\mathbf n$  vectors (Nmax) is sufficient for a rapid convergence. On the other hand, a small  $\kappa$  causes the reciprocal-space sum to converge fast since as  $\kappa \to 0$ , the  $\exp(-x/\kappa) \to 0$ , that is, a small number of vectors in K-space (KSQmax) will be enough.

Within the accurate calculation range, the potential energy is invariant to the choice of  $\kappa$ . This can be used as a testing principle to verify the Ewald summation code.

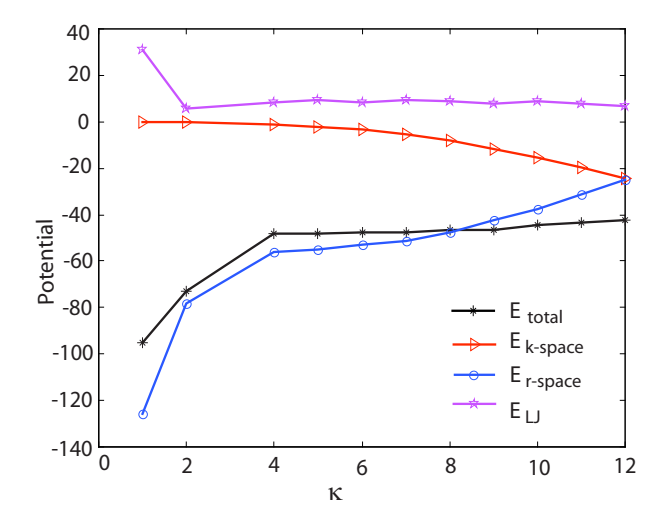


FIGURE 3.4. Potential energy of bulk water calculated as the function of  $\kappa$ . The temperature is 300 K; the number of water molecules is 256; Nmax=7; KSQmax=50, more than 600 vectors in K-space are used.

Figure 3.4 shows the potential of energy of a bulk water system containing 256 water molecules. The relationship of these potentials is,

$$V_{total} = V_{LJ} + V_R + V_K, (3.32)$$

where  $V_{total}$  is the total potential energy, and  $V_{LJ}$  is the Lennard-Jones potential [see expression (2.42)], and  $V_R$  is the real space potential and  $V_K$  is the K-space potential [see expression (3.28)]. From Figure 3.4, we observe that when  $\kappa$  in the value interval of  $4 \sim 8$ , the total potential calculated is invariant. The total potential is round 46 KJ/mol, which is consistent with the work of English & Macelroy (2002). In our calculations,  $\kappa$  always takes the value of 5.

#### CHAPTER 4

# Simulation results

Currently DEP is generally used for separation and manipulation micro and nanoparticles in biochemistry and mechanical engineering due to its demonstrated simplicity and high selectivity [Morgan & Green (2003); Krupke  $et\ al.$  (2003a)]. Here we present some of our numerical simulations for manipulating E.coli bacteria, micro particles and SWNTs by DEP force, a model to numerically calculate the DEP force acting on rod-like particles, and a MD study of dielectric properties of water confined in SWNTs.

## 4.1. Superimposition of dielectrophoretic forces

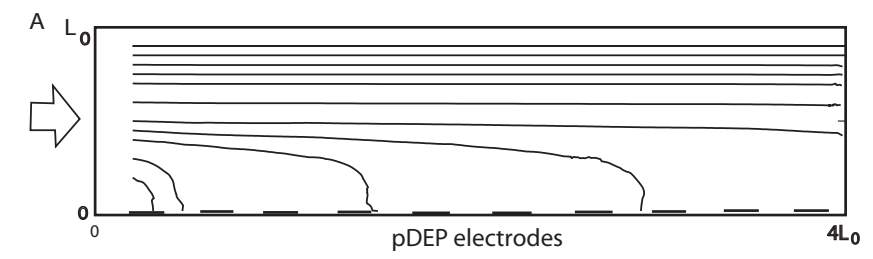
In one of our previous studies [Aldaeus et al. (2005)], superimposed DEP forces are used to improve the efficiency of trapping *E.coli* bacteria.

Figure 4.1 shows the traces of E.coli bacteria under DEP forces in a rectangular channel. Three different electrode configurations are considered (see Figure 4.1). A Poiseuille flow enters the channel from the left. Particles are released from different heights through the channel cross section. In configuration A shown in Figure 4.1(a), only the electrodes at the bottom of the channel are used. The frequency of the AC field is chosen to give a positive DEP, i.e., particles are attracted to regions of high field gradients. In configuration B shown in figure 4.1(b), both the electrodes at the bottom and the top were turned on at a voltage frequency where the particles only obtain a positive DEP motion. In configuration C shown in figure 4.1(c), both the electrodes are turned on, but different frequencies are utilized. The bottom electrodes have a frequency inducing positive DEP, and the top electrodes have a frequency inducing negative DEP. The trapping rate of configuration B is 100%, which proves that configuration B is the best one in this condition.

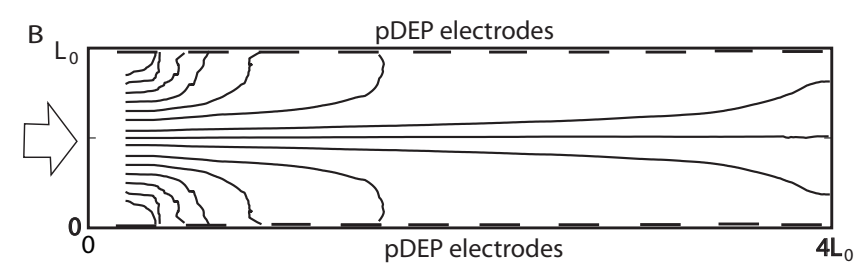
## 4.2. Multi-step dielectrophoresis

The idea of multi-step DEP is, by repeating the trapping-release pocess, particles with small difference in size and/or dielectric properties can be separated [Aldaeus et al. (2006)].

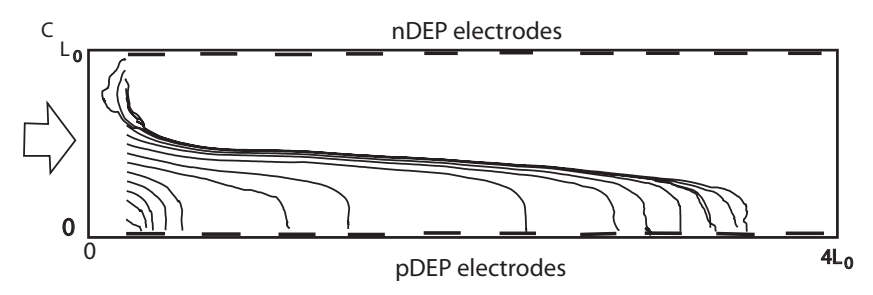
Figure 4.2(a) is the schematic diagram of this strategy, where two groups of particles, X and Y are observed to be completely separated after a number of repeating trapping-release steps.



(a) performed in the pDEP mode at the bottom.



(b) with pDEP both at the bottom and at the top.



(c) with pDEP at the bottom and nDEP at the top.

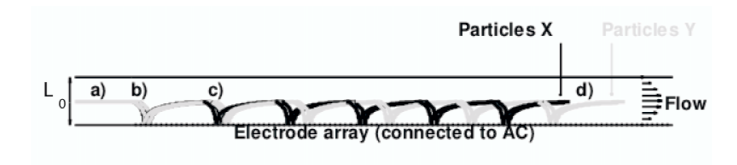
FIGURE 4.1. Particle trajectories in a high conductivity solution.

To quantify the degree of fractionation, a concept as the dielectrophoretic resolution  $(R_{DEP})$  is defined as

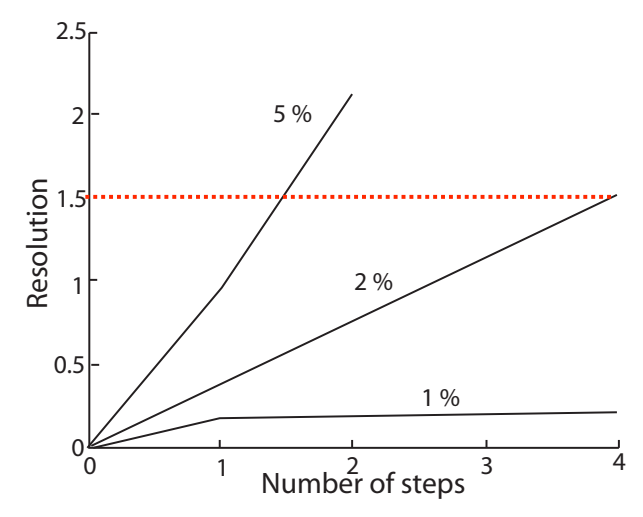
$$R_{DEP} = \frac{3d}{w_A + w_B} \tag{4.1}$$

where d is the distance between the two centers of each particle population, and w is the band width of the particle population. It is easy to understand that when  $R_{DEP} > 1.5$ , the two particle populations will be completely separated, because it is equivalent to

$$d > \frac{w_a + w_b}{2}.\tag{4.2}$$



(a) The schematic of the experiment principle. Two groups of particles with small difference are separated after multi-step trapping and releasing.



(b) Calculated resolution as a function of number of steps for a relative difference in size of 5%, 2% and 1%.

FIGURE 4.2. Multi-step dielectrophoresis analysis.

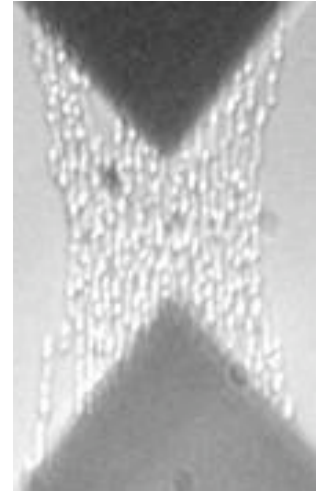
For example, Figure 4.2(b) shows that a complete separation can be achieved after two steps if the difference in size is 5%. If the size difference is 2%, four steps are required.

### 4.3. Inter-particle dielectrophoretic forces

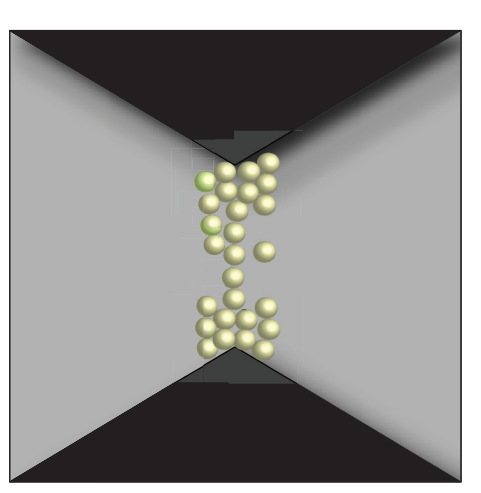
To simulate the motion particles in detail, it is essential to include all the other important forces acting on the particle besides DEP, i.e. the repulsive force from the wall, the repulsive force from the interface of other particles, the hydrodynamic forces and the inter-particle electrostatic force due to the induced charges. Based on the model, we simulated the motion of the  $E.\ coli$  bacteria under DEP force and the result is comparable to the experiment observation.

Figure 4.3(a) shows an experimental result of E. coli bacteria under positive DEP force. The electrodes are seen as the v-shaped structures at top and

bottom. The bacteria accumulate near the electrode tips, as expected, since these are the points with the largest field gradients. Furthermore they organize into long chains, extending along the electric field lines. This is due to the fact that, under the present conditions, with an AC frequency giving positive DEP, the particles polarize in such a way that they will be negatively charged at the end near the positive electrode, and vice versa. This will create attractive inter-particle forces between these induced dipoles. Finally the particles form the long chains along the electric field lines. Figure 4.3(b) shows the simulation and which is in good agreement with the experimental result.



(a) Experimental observation of E.coli bacteria under DEP force.



(b) Simulation results of micro particles under DEP force.

FIGURE 4.3. Comparison of numerical simulation and experimental observation. Under positive DEP forces, the particles are attracted to the tip of triangular electrodes. The *pearl chains* are formed due to the interaction between the particles caused by the induced charges.

### 4.4. Electrothermal flow in DEP separation of SWNTs

Separating metallic and semiconducting carbon nanotube by DEP was suggested by Krupke et~al.~(2003a) and attracted extensive research and application interests [Krupke et~al.~(2004); Zhang et~al.~(2006); Dimaki & Bøggild (2004)]. In many experiments of DEP separation of SWNTs, both metallic and semi-conducting SWNTs are observed to be attracted to the electrodes although they process remarkably different electric properties [Krupke et~al.~(2004); Zhang et~al.~(2005)]. A likely explanation is that the motion of SWNTs

### 4. SIMULATION RESULTS

are affected by electric field-driven fluid flows, for instance, the electrothermal flow due to the joule heating by the gradient of electric field [Lin et al. (2007)], which was observed in micro system experiments [Ramos et al. (1998); Green et al. (2002)].

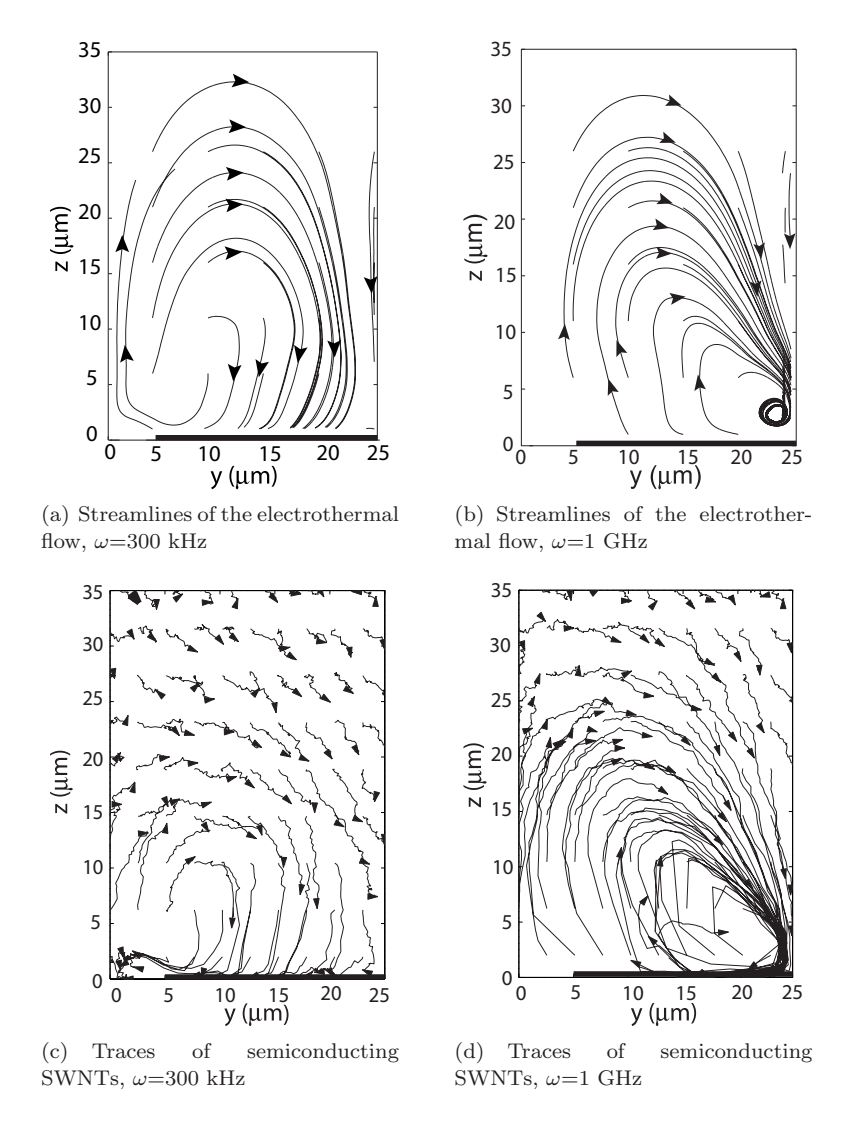


FIGURE 4.4. Streamlines and corresponding traces of semi-conducting SWNTs in 0.1% SDBS solutions, low (300 kHz) and high (1 GHz) frequency regimes with  $\phi$ =20 V.

In one of our works (see Figure 4.4), the electrothermal fluid flow is calculated by solving the incompressible Navier-Stokes equation with the external electrothermal force. The velocities of semiconducting SWNTs are calculated as the result of the sum of the DEP force, Brownian motion and the electrothermal forces. The simulation show that within a certain electric potential range, in the domain closed to the electrodes, DEP force is the dominating force, and far from the electrodes, Brownian motion is dominating. In the intermediate rather large domain, the traces of SWNTs agree with the electrothermal flow streamlines well. Since the electrothermal flow is frequency-dependent, the pattern of streaming lines of the flow are rather different in low and high frequency ranges.

# 4.5. Calculation of DEP force on a slender body

The assumption of the widely employed effective dipole moment is that the length scale of the particle should be much less than that of the geometry and this is not true for a rod-like particle (carbon nanotubes, virus, DNA etc). Therefore, a new model is formulated to numerically calculate the DEP force of a dielectric straight slender body immersed in a dielectric medium. The idea is to approximate the slender body by a prolate ellipsoid, and assume that the induced charges are concentrated along the centerline. This model is applicable when the shape parameter, slenderness  $\delta$  (the max rate of the radius of the ellipsoid to the length of the ellipsoid) is much less than one. The unknown induced charge densities are calculated by enforcing the boundary conditions.

We consider an ellipsoid immersed into a medium, with the relative permittivity ratio between particle and the medium to be 20. The calculations by effective dipole moment and by the presented method are both carried out for comparison shown in Figure 4.5. The length and the slenderness of ellipsoid are varied to obtain the effects on the differences. It is apparently observed that when the length of tube increases, the difference between the results of the two methods increases, and when the slenderness was reduced, the differences increased.

### 4.6. Dielectric properties of water inside SWNTs

The dynamic properties of water confined in nanoscale geometries are expected to dramatically differ from those of bulk water. It is essential for biochemistry to understand those properties since such water actually exists in the surroundings and within our bodies. Besides, water-filled carbon nanotubes are expected to play a central role in future nanoscale devices, for proton storage and transport applications [Mann & Halls (2003)]. MD simulations are carried out to study the dielectric properties of water inside single-walled carbon nanotubes. The interaction between water molecules is modeled by the extended

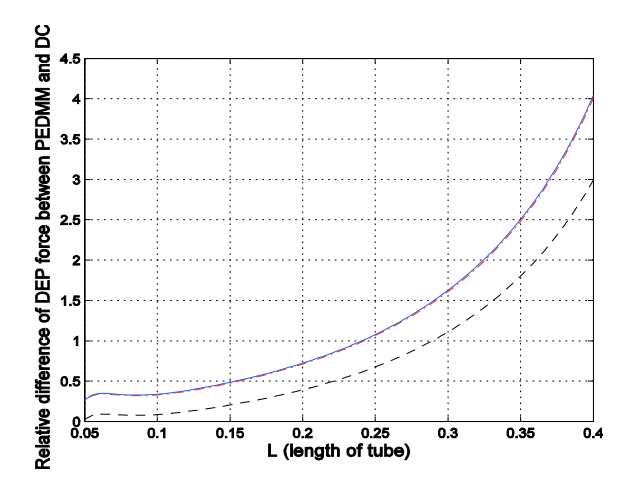


FIGURE 4.5. Relative difference in magnitude of DEP forces calculated by the effective dipole moment method and the distributed charge method. Solid line:  $\delta = 0.001$ , dash-dot line(which is almost on top of the solid line):  $\delta = 0.01$ , dash line:  $\delta = 0.1$ . The gap between electrode is 0.4 L, and the permittivity ratio  $\epsilon = 20$ .

single point charge (SPC/E), and the interactions between carbon atoms are modeled by Brenner potentials.

The static and dynamic dielectric properties of water are calculated within carbon nanotubes with various radii. The results show that along axial direction, the static dielectric permittivity and relaxation time are larger than those of isotropic bulk water, and in the cross-section plane, it is the opposite. Therefore, concerning the full dynamic permittivity, the water confined has two dielectric relaxation frequencies differing from the one relaxation frequency which bulk water has (see Figure 4.6). The smaller the radius, the larger the difference is.

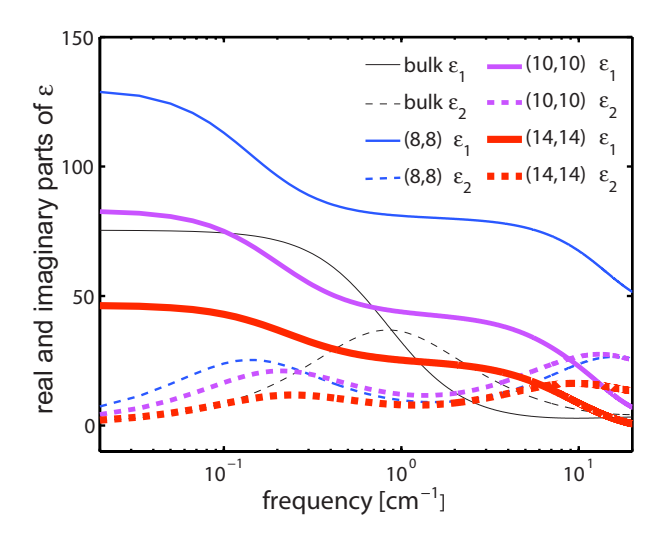


FIGURE 4.6. Dynamic dielectric permittivity of water confined in SWNTs and bulk water.  $\epsilon_1$ : the real part of permittivity;  $\epsilon_2$ : the imaginary part of permittivity.

#### CHAPTER 5

# Conclusions and outlooks

The work presented in this thesis concerns several aspects in the modeling of DEP in micro and nano systems: modeling of the DEP force acting on micro and nano particles; fluid dynamics in DEP systems; dielectric properties of water confined in an armchair SWNT. The numerical aspects concerned are mainly the finite element method and MD method. Finite element method toolboxes, FemLego and Comsol Multiphysics are used to numerically solve the Navier Stokes equations with the electrothermal force and the DEP force respectively. The MD code written in Fortran90 is original developed by Maruyama Lab of Department of Mechanical Engineering, University of Tokyo.

Based on the effective dipole moment to calculate DEP force, the particle dynamics model solves the equations of motions of particles step-by-step. The interaction between particles due to the induced dipoles and the hydrodynamic forces can be included into the calculation as well. This method with the interactions neglected is used to calculate DEP motions of particles in a micro channel with a carrier Poiseuille flow. The first application shows that superimposed external electric fields can greatly enhanced the trapping rate of E. Coli bacteria. The second application reveals that by using this multi-step trapping-releasing mechanism, particles with much smaller difference in size and dielectric properties can be separated, than in traditional ways. Concerning the Brownian motion and electrothermal flow, this model is modified to calculate the motion of semiconducting SWNTs, and the results show that the Brownian motion, DEP force and electrothermal flow have their voltage and frequency dependent dominating domain.

When the length of rod-shaped particles is comparable to the length scale of the geometry, the assumption of effective dipole moment method for DEP force is not true. Therefore, a new model based on one-dimensional induced charge density is suggested to numerically calculate the DEP force instead of the effective dipole moment method, and it is expected to provide results with higher accuracy. Compared to Maxwell stress tensor, its computation work is much cheaper and electrostatic interactions between particles is easy to implement.

The dielectric properties of water confined in SWNTs are studied by MD simulations. Strong anisotropy is observed due to the orientational alignment

of water molecules, and the anisotropy is also radius-dependent. Density and length effects to the dielectric properties of confined water are also studied.

In future work, the molecular dynamics code can be directly employed to calculate other systems, for example, the dynamic properties of water on the surface of carbon nanotube bundles. If the flexible simple point charge model for water molecule is used instead of SPC/E, the vibration spectrum can be calculated too, and the dielectric constant in higher frequency range can also be obtained.

Combining the method of calculating hydrodynamic forces of many interacting rigid fibers by slender body theory suggested by Tornberg & Gustavsson (2006) with our current distributed charge method which numerically calculates DEP force acting on rod-shaped particles, electric interactions can also be added.

The finite element method can be used to simulate the DEP motion of finite size particles. For example, rigid particles in a fluid can be described by independent solid meshes moving in fixed background meshes, and the fluid flow containing rigid particles can be solved by the distributed Lagrange multipliers method suggested by Glowinski *et al.* (2001). As for deformable particles, i.g., bio-cells or droplets, phase field or level set method can be used to simulate the dynamic interfaces.

We have discussed the important role that the electrokinetic transport plays in terms of the electrothermal flow in the DEP separation of SWNTs. In paper 4, we show that the electrothermal flow can dominate the motion of SWNTs in certain conditions. Electrothermal flow has not been studied to the same extent as some other electrokinetically driven flows. It would be interesting to explore other situations where electrothermal flow maybe important. As pointed out by Morgan & Green (2003), AC electroosmosis dominates the flow motion in low frequency range. Therefore, when the frequency of the applied AC electric field of DEP systems is within this range, it is interesting and necessary to study the motion of the AC electroosmosis flow and investigate how the AC electroosmosis flow affects the motion of particles.

Electro kinetically driven micro flows have been generally observed in experiments and act as important micro flow control mechanisms as well as pressure [Karniadakis & Beskok (2001)]. Correctly simulating the electrokinetic flows would be very useful to demonstrate the electric field-driven flow control in complex micro geometries. By including the calculation of presented electrokinetic flow, the DEP systems can also be more accurately simulated.

# Acknowledgements

Many thanks and the deepest appreciation to my supervisor Professor Gustav Amberg for offering me the opportunity to do interesting PhD studies, for always providing resourceful helps with his abundant knowledge, keen insights to physical phenomena and great patience. Also many thanks to Dr. Junichiro Shiomi for introducing me into the field of molecular dynamics, for the hardworking and relaxing time together. Many thanks to Professor Maruyama Shiego for the fruitful and pleasant visit at the University of Tokyo. Thanks to Dr. Fredrik Aldaeus and Professor Johan Roeraade at Department of Chemistry, for nice collaborations in dielectrophoretic separation of micro particles. Thanks to Professor Shi-li Zhang and Dr. Zhi-bin Zhang for stimulating discussions. Thanks to Dr. Luca Brandt for reviewing and commenting on my thesis.

Many thanks to the staffs at Department of Mechanics for contributing a comfortable and enjoyable study and working atmosphere. Especially, Minh Do-Quang, Walter Villanueva, Tobias Strömgren, Andreas Vallgren, Ali Farzadi in our research group are thanked for sharing their knowledge and some of them have been my former and current officemates. Thanks to Jerome Hoepffner, Nulifer Ipek, Shiho Tanaka for pleasant conversations. Thanks to Pär Ekstrand for taking care of computer systems. Thanks to Ingunn Wester for handling my numerous documents.

I also wish to express my gratitude to all my friends in China, Sweden and Japan and to the unknown people who helped me. Deep thanks to my father Feng-Chuan Lin and my mother, Yu-Xiu Ye who have constantly been encouraging and supporting me. Lastly and most importantly, I want to thank my husband, Ming Xiao for his love and companies.

The Swedish Research Council (VR) is gratefully acknowledged for the financial support, and Swedish National Infrastructure for Computing (SNIC) is thanked for computer resources.

# **Bibliography**

- ALBE, K., NORDLUND, K. & AVERBACK, R. S. 2002 Modeling the metal-semiconductor interaction: Analytical. *Phys Rev B* **65**, 195124(1–5).
- ALDAEUS, F., LIN, Y., AMBERG, G. & ROERAADE, J. 2006 Multi-step dielectrophoresis for separation of particles. *Journal of Chromatography A* **1131**, 261–266
- ALDAEUS, F., LIN, Y., ROERAADE, J. & AMBERG, G. 2005 Superpositioned dielectrophoresis for enhanced trapping efficiency. *Electrophoresis* **26**, 4252–4259.
- ALLEN, M. P. 2004 Computational Soft Matter: From Synthetic Polymers to Proteins, Lecture Notes. John von Neumann Institute for Computing, Julich.
- ALLEN, M. P. & TILDESLLEY, D. J. 1987 Computer Simulation of Liquids. Oxford Science Publication.
- Amberg, G., Tönhardt, R. & Winkler, C. 1999 Finite element simulations using symbolic computing. *Math. Comp. Simulation* **49**, 257–274.
- Anderson, J., Ullo, J. J. & Yip, S. 1987 Molecular dynamics simulation of dielectric properties of water. *Journal of Chemical Physics* 87, 1726–1733.
- ASAMI, K. H. & KOIZUMI, T. N. 1980 Dielectric analysis of escherichia coli suspensions in the light of the theory of interfacial polarization. *Journal of Biophys* 31, 215–228.
- Asbury, C. L. & Engh, G. V. D. 1998 Trapping of dna in nonuniform oscillating electric fields. *Biophysical Journal* 74, 1024–1030.
- Barshinger, R. & Geer, J. 1987 The electrostatic field about a slender dielectric body. SIAM J. Appl. Math. 47, 605–623.
- Batchelor, G. K. 1970 Slender-body theory for particles of arbitrary cross-section in stokes flow. *Journal of fluid mechanics* 44, 419–440.
- Becker, F. F., Wang, X., Huang, Y., Pethig, R., Vykoukal, J. & Gascoyne, P. R. C. 1995 Separation of human breast cancer cells from blood by different dielectric affinity. *Proc. Natl. Acad. Sci. USA*. **82**, 860–864.
- Berendsen, H. J. C., Grigera, J. R. & Straatsma, T. P. 1987 The missing term in effective pair potentials. *J. Phys. Chem. B* **91**, 6269–6271.
- Brenner, D. W. 1990 Empirical potential for hydracarbons for use in simulating the chemical vapor deposition of diamond films. *Physical Review B* **42** (15), 9458–9471.

- Castellanos, A., Ramos, A., González, A., Green, N. G. & Morgan, H. 2003 Electrohydrodynamics and dielectrophoresis in microsystems: scaling laws. *J. Phys.: D Appl. Phys.* **36**, 2584–2597.
- DIMAKI, M. & BØGGILD, P. 2004 Dielectropohoresis of carbon nanotubes using microelectrodes: an numerical study. *Nanotechnology* **15**, 1095–1102.
- ELIMELECH, M., GREGORY, J., JIA, X. & WILLIAMS, R. A. 1995 Particle Deposition and Aggregation Measurement, Modelling and Simulation. USA: Elsevier.
- English, N. J. & Macelroy, J. M. 2002 Atomistic simulations of liquid water using lekner electrostatics. *Molecular physics* **100** (23), 3753–3769.
- Feldman, H. C., Sigurdson, M. & Meinhart, C. D. 2007 Ac electrothermal enhancement of heterogeneous assays in microfluidics. *Lab on a Chip* 7, 1553–1559.
- GASCOYNE, P. R. C., WANG, X. B., HUANG, Y. & BECKER, F. F. 1997 Dielectrophoretic separation of cancer cells from blood. *IEEE transactions on industry applications* 33, 670–678.
- GEER, J. 1976 Stokes flow past a slender body of revolution. *J. Fluid Mech* 78, 577–600.
- GLOWINSKI, R. P., PAN, T. W., HESLA, T. I., JOSEPH, D. D. & PERIAUX, D. D. 2001 A fictious domain approach to the direct numerical simulation of incompressible application to particulate flow. *J. Computational Physics* **169**, 363–426.
- GORDILLO, M. C. & MARTI, J. 2002 Molecular dynamics description of a layer of water molecules on a hydrophobic surface. *Journal of Chemical Physics* 117, 3425–3430.
- GORDILLO, M. C. & MARTI, J. 2003 Water on the outside of carbon nanotube bundles. *Physical Review B* **67**, 205425(1–4).
- Green, N. G. & Morgan, H. 1999 Dielectrophoresis of submicrometer latex spheres. i: Experimental results. *J. Phys. Chem. B* **103**, 41–50.
- Green, N. G., Morgan, H. & Milner, J. J. 1997 Manipulation and trapping of sub-micron bioparticles using dielectrophoresis. *J. Biochemical and Biophysical Methods* 35, 89–102.
- Green, N. G., Ramos, A. & Morgan, H. 2002 Fluid flow induced by nonuniform ac electric fields in electrolytes on microelectrodes. i.experimental measurements. *J. Electrostatics* **56**, 235–254.
- Gregory, J. K., Clary, D. C., Liu, K., Brown, M. G. & Saykally, R. J. 1997 The water dipole moment in water clusters. *Science* 275 (5301), 814–817.
- GUILLOT, B. 2002 A reappraisal of what we have learnt during three decades of computer simulations on wate. J Mol. Liq. 101, 219–260.
- Helvajian, H., ed. 1999 Microengineering Aerospace Systems. American Institute of Aeronautics and Ast.
- Heyes, D. M. 1984 Md incorporating ewald summations on partrial charge polyatomic systems. ccp5 NewsLetters .
- ${\tt Jones,\ T.\ B.\ 1995}\ \textit{Electromechanics\ of\ Particles}.\ {\tt UK:\ Cambridge\ University\ Press}.$
- JONES, T. B. & WASHIZU, M. 1996 Multipolar dielectrophoretic and electrorotation theory. J. Electrostatics 37, 121–134.

- KADAKSHAM, J., SINGH, P. & AUBRY, N. 2004 Dielectrophoresis of nanoparticles. *Electrophoresis* **25**, 3525–3632.
- Kadaksham, J., Singh, P. & Aubry, N. 2005 Manipulation of particles using dielectrophoresis. *Mechanics Research Communications* **33**, 208–122.
- Karniadakis, G. E. & Beskok, A. 2001 Micro flows: fundamentals & simulation. Springer.
- KRUPKE, R., HENNRICK, F., KAPPES, M. M. & LÖHNEYSEN, H. V. 2004 Surface conductance induced dielectrophoresis of semiconducting single-walled carbon nanotubes. *Nano Lett.* 4, 1395.
- KRUPKE, R., HENNRICK, F., LÖHNEYSEN, H. V. & KAPPES, M. M. 2003a Separation of metallic from semiconducting single-walled carbon nanotubes. *Science* **301**, 344.
- KRUPKE, R., HENNRICK, F., WEBER, H. B., KAPPES, M. M. & LÖHNEYSEN, H. V. 2003b Simultaneous deposition of metallic bundles of single-walled carbon nanotubes using ac-dielectrophoresis. *Nano Letter* 3, 1019–1023.
- KRUPKE, R., LINDEN, S., RAPP, M. & HENNRICH, F. 2006 Thin films of metallic carbon nanotubes prepared by dielectrophoresis. *Adv. Mat.* **18**, 1468–1470.
- Laasonen, K., Sprik, M., Parrienello, M. & Car, R. 1993 Ab initio liquid water. J. Chem. Phys. 90, 9080.
- LEEUW, S. W. D., PERRAM, J. W. & SMITH, E. R. 1980 Simulation of electrostatic systems in periodic boundary conditions. i. lattice sums and dielectric constants. *Proc. R. Soc. Lond. A.* **373**, 27–56.
- Liang, E., Smith, R. L., & Clague, D. S. 2004 Dielectrophoretic manipulation of finite sized species and the importance of the quadrupolar contribution. *Phys. Rev. E* **70**, 066617(1–8).
- LIN, Y., SHIOMI, J., MARUYAMA, S. & AMBERG, G. 2007 Electrothermal flow in dielectrophoresis of single-walled carbon nanotubes. *Physical Review B* **76**, 045419–045423.
- Lyklema, J. 1995 Fundamentals of Interface and Colloid Science ii. UK: London Academic.
- Mann, D. J. & Halls, M. D. 2003 Water alignment and proton conduction inside carbon nanotubes. *Phys. Rev. Lett.* **90**, 195503(1–4).
- Markx, G. H., Dyda, P. A. & Pethig, R. 1996 Dielectrophoretic separation of bacteria using a conductivity gradient. *J. Biotechnology* **51**, 175–180.
- MARKX, G. H., PETHIG, R. & ROUSSELET, J. 1997 The dielectrophoretic levitation of latex beads, with reference to field-flow fractionation. *J. Physics* **30**, 2470–2477.
- Marti, J. & Gordillo, M. C. 2001 Time-dependent properties of liquid water isotopes absorbed in carbon nanotubes. *Journal of Chemical Physics* **114**, 10486–10402
- Marti, J. & Gordillo, M. C. 2002 Effects of confinement on the vibrational spectra of liquid water adsorbed in carbon nanotubes. *Physical Review B* **63** (165430).
- Marti, J., Guardia, E. & Padro, J. A. 1994 Dielectric properties and infrared spectra of liquid water: Influence of the dynamic cross corrections. *Journal of Chemical Physics* **101**, 10883–10891.

- Marti, J., Nagy, G., Guardia, E. & Gordillo, M. C. 2006 Molecular dynamics simulation of liquid water confined inside graphite channels: dielectric and dynamical properties. *Journal of Phys. Chem. B* **110**, 23987–23994.
- MORGAN, H. & GREEN, N. G. 1997 Dielectrophoretic manipulation of rodshaped viral particles. *J. Electrostatics* **42**, 279–293.
- MORGAN, H. & GREEN, N. G. 2003 AC Electrokinetics: Colloids and Nanoparticles. England: Research Studies.
- Morgan, H., Green, N. G., Hughes, M. P., Monaghan, W. & Tan, T. C. 1997 Large-area travelling-wave dielectrophoresis particle separation. *J. Micromechanics and Microengineering* **7**, 65–70.
- Müller, T., Gerardino, A., Schnelle, T., Shirley, S. G., Bordoni, F., De, G. G., Leoni, R. & Fuhr, G. 1996 Trapping of micrometre and sub-micrometre particles by high-frequency electri fields and hydrodynamic forces. *Phys. D: Appl. Phys.* 29, 340–349.
- Pearlmana, D. A., Caseb, D. A., Caldwelle, J. W., Rosse, W. S., Cheatham, T. E., Deboltb, S., Fergusond, D., Seibele, G. & Kollman, P. 1995 Amber, a package of computer programs for applying molecular mechanics, normal mode analysis, molecular dynamics and free energy calculations to simulate the structural and energetic properties of molecules. *Computer Physics Communications* 91, 1–14.
- Pohl, H. A. 1975 Dielectrophoresis. Cambridge University Press.
- Popović, B. D. 1971 Introductory engineering electromagnetics. Addison Wesley.
- Ramos, A., Morgan, H., Green, N. G. & Castellanos, A. 1998 Ac electrokinetics: a review of forces in microelectrode structures. *Phys. D: Appl. Phys.* **31**, 2338–2353.
- Refson, K. 2001 Moldy User's Manual.
- ROSALES, C. & Lim, K. M. 2005 Numerical comparison between maxwell stress method and equivalent multipole approach for calculation of the dielectrophoretic force in single-cell traps. *Electrophoresis* **26**, 2057–2065.
- Sadus, R. J. 1999 Molecular simulation of fluid: theory, algorithms and objectorientation. Elsevier, Neitherland.
- Saito, R., Dresselhaus, G. & Dresselhaus, M. S. 1998 *Physical Properties of Carbon Nanotube*. London: Imperial College.
- Sellier, A. 2001 A slender dielectric body embedded in an arbitrary external potential. *J. Appl. Math.* **66**, 149–173.
- Shoemake, K. 1985 Animating rotation with quaternion curves. ACM Siggraph Computer Graphics 19, 245–254.
- Singh, P. & Aubry, N. 2007 Transport and deformation of droplets in a microdevice using dielectrophoresis. *Electrophoresis* **28**, 644–657.
- STRATTON, J. A. 1941 Electromagnetic theory. McGraw-Hill Book company.
- Todorov, I. T. & Smith, W. 2006 THE DL POLY 3 USER MANUAL. Cheshire, UK.
- TORNBERG, A.-K. & GUSTAVSSON, K. 2006 A numerical method for simulations of rigid fiber suspensions. *Journal of Computational Physics* **215**, 172–196.

- Tuukkanen, S., Kuzyk, A., Toppari, J., Häkkinen, H., Hytönen, V. P., Niskanen, E., Rinkiö, M. & Törmä, P. 2007 Trapping of 27 bp 8 kbp dna and immobilization of thiol-modified dna using dielectrophoresis. *Nanotechnology* **18**, 295204–295214.
- Wang, X.-J., Wang, X.-B. & Gascoyne, P. R. C. 1997 General expressions for dielectrophoretic force and electrorotational torque derived using the maxwell stress torque. *J. Electrostatics* **39**, 277–295.
- Washizu, M. 1992 Precise calculation of dielectrophoretic force in arbitrary field. J. Electrostatics **27**, 177–188.
- Washizu, M. 2004 Equivalent multipole-moment theory for dielectrophoresis and electrorotation in electromagnetic field. *J. Electrostatics* **62**, 15–33.
- Washizu, M. & Jones, T. B. 1994 Multipolar dielectrophoretic force calculation. J. Electrostatics 33, 187–198.
- Washizu, M. & Kurosawa, O. 1990 Electrostatic manipulation of dna in microfabricated structures. *IEEE Trans. Ind. Electron.* **26** (1165), 1990.
- Washizu, M., Suzuki, S., Kurosawa, O., Nishizaka, T. & Shinohara, T. 1994 Molecular dielectrophoresis of biopolymers. *IEEE Trans. on Ind. Appl.* **30**, 835–843
- WATANABE, K. & KLEIN, M. L. 1989 Effective pair potentials and the properties of water. *Chem. Phys.* **131**, 157.
- Yang, J., Huang, Y., Wang, X. B., Becker, F. F. & Gascoyne, P. R. C. 1999 ell separation on microfabricated electrodes using dielectrophoretic gravitational field-flow-fraction", *Analytical Chemistri* 71, 911–918.
- Zhang, Z.-B., Liu, X.-J., Zhang, S.-L. & Campbell, E. E. B. 2005 Alternating current dielectrophoresis of carbon nanotubes. *J. Appl. Phys.* **98**, 056103.
- Zhang, Z.-B., Zhang, S.-L. & Campbell, E. E. B. 2006 Dielectrophoretic behavior of ionic surfactant-solubilized carbon nanotubes. *Chem. Phys. Lett.* **421**, 11–15.

Part II

Papers